Spin tunneling and phonon-assisted relaxation in Mn_{12}-acetate

Michael N. Leuenberger* and Daniel Loss†
Department of Physics and Astronomy, University of Basel, Klingelbergstrasse 82, 4056 Basel, Switzerland
(Received 13 July 1999)

We present a comprehensive theory of the magnetization relaxation in a Mn_{12}-acetate crystal in the high-temperature regime ($T \gtrsim 1$ K), which is based on phonon-assisted spin tunneling induced by quartic magnetic anisotropy and weak transverse magnetic fields. The overall relaxation rate as function of the longitudinal magnetic field is calculated and shown to agree well with experimental data including all resonance peaks measured so far. The Lorentzian shape of the resonances, which we obtain via a generalized master equation that includes spin tunneling, is also in good agreement with recent data. We derive a general formula for the tunnel splitting energy of these resonances. We show that fourth-order diagonal terms in the Hamiltonian lead to satellite peaks. A derivation of the effective linewidth of a resonance peak is given and shown to agree well with experimental data. In addition, previously unknown spin-phonon coupling constants are calculated explicitly. The values obtained for these constants and for the sound velocity are also in good agreement with recent data. We show that the spin relaxation in Mn_{12}-acetate takes place via several transition paths of comparable weight. These transition paths are expressed in terms of intermediate relaxation times, which are calculated and which can be tested experimentally.

I. INTRODUCTION

The magnetization relaxation in the molecular magnet Mn_{12}-acetate with chemical formula, $[Mn_{12}(CH_3COO)_{16}(H_2O)_4O_{12}]\cdot 2CH_3COOH\cdot 4H_2O$ (henceforth abbreviated as Mn_{12}) has attracted much recent interest since several experiments[1–5] have indicated unusually long relaxation times — about two months at a temperature of about 2 K — as well as pronounced peaks in the relaxation time[6–8] in response to a varying magnetic field H_z when applied along the easy axis of the Mn_{12} crystal. These peaks correspond to an increased relaxation rate of the magnetization of Mn_{12} and occur when H_z is tuned to multiples of about 0.44 T. According to earlier suggestions[9,10] this phenomenon has been interpreted as a manifestation of resonant tunneling of the magnetization, often referred to as macroscopic quantum tunneling (MQT). A qualitative explanation goes as follows. From the microscopic point of view a Mn_{12} cluster acts like a giant spin with length $s=10$ as long as the external magnetic field is small compared to the exchange interactions between the Mn ions, which is fulfilled in the experimental range considered in this paper. The relaxation rate of the magnetization increases at field values where the spin states become pairwise degenerate. It is this degeneracy that determines the resonance condition. As the external field H_z is moved away from a resonance the spin states are no longer perfectly degenerate, and therefore the tunneling probability becomes smaller and thus the relaxation rate. Since the spin system couples to the environmental phonons of the Mn_{12} crystal, the energy levels of the spin states are smeared out. This leads to homogeneously broadened resonance peaks that are of Lorentzian shape. There are also other sources which lead to broadening of the resonances, such as hyperfine and dipolar fields.[11] They give rise to inhomogeneous broadening with Gaussian-shaped peaks.[12,13] However, this stands in contrast to the measured resonance peaks, which are nearly perfect Lorentzians.[11] Furthermore, the width of the hyperfine induced Gaussians[12,14] turns out to be smaller for $T \gtrsim 1$ K than the width of the Lorentzians obtained below and seen in the experiment.[15] Similarly, dipolar interactions have been ruled out by experiments on diluted samples.[16] Thus, for temperatures $T \gtrsim 1$ K we can safely neglect hyperfine and dipolar fields, and the dominant source of the peak broadening can be explained consistently by spin-phonon effects only.

In a critical comparison between model calculations[12,14,17–20] and experimental data[6,7,11] Friedman *et al.*[11] point out that a consistent explanation of the experimentally observed relaxation is still missing. A good starting point for theoretical calculations has been formulated by Villain *et al.*,[17] where the relaxation is described in terms of spin-phonon interaction and a generalized Orbach process. However, this approach does not include the dependence on the external field H_z. Also, one of the main challenges for theory is to explain the overall shape of the relaxation curve as well as the nearly perfect Lorentzian shape of the measured resonance peaks.[11]

In this work we perform a model calculation of the magnetization relaxation which is based on phonon-assisted tunneling. We present a self-consistent theory which is in reasonably good agreement both with the overall relaxation rate (including all resonances) measured by Thomas *et al.*[7] (see Fig. 3) and with the Lorentzian shape of the first resonance peaks (see Figs. 7 and 8) measured by Friedman *et al.*[11] with high precision for four different temperatures.

Our model, which is introduced in Sec. II, contains five independent parameters: three anisotropy constants $A \gg B \gg B_4$, the misalignment angle θ (angle between field direction and easy axis, the latter being taken along the z axis), and the sound velocity c. The anisotropy constant B_4 and the angle θ are responsible for the spin tunneling. This will be explained in Sec. III. Moreover, we derive the spin-phonon coupling constants in Sec. II. It turns out from our calculations that these constants can be expressed in terms of the

anisotropy A. The constants A,B,B_4 have already been measured[21,22] and are known within some experimental uncertainty. We achieve optimal agreement between our theory and data if we proceed as follows. In accordance with Ref. 11 we set $\theta=1°$, while the constants A,B,B_4 are fitted to the relaxation data by observing, however, the constraints that A,B,B_4 are allowed to vary only within the range of their experimental uncertainties. The sound velocity c has not been directly measured yet (to our knowledge). However, specific heat measurements[42] yield the Debye temperature of Mn_{12}, from which a sound velocity can be deduced that is in excellent agreement with our fit of the sound velocity $c=(1.45-2.0)\times 10^3$ m/s (see Sec. IV). Thus, in contrast to previous results[12,14,17–19] our theory is in reasonably good agreement not only with the relaxation data[7,11] but also with *all* experimental parameter values known so far (see Figs. 3, 7, and 8). In addition, predictions are made which can be tested experimentally: the sound velocity c and the intermediate relaxation times τ_n, as well as satellite peaks.

In Sec. III, extending previous work,[12,14,17–19] we make use of a generalized master equation which treats phonon-induced spin transitions between nearest and next-nearest energy levels as well as resonant tunneling due to quartic anisotropies and transverse fields on the same footing, which results in the Lorentzian shape of the resonances. We derive the effective linewidth of the Lorentzian peaks (see Sec. VI) as well as a generalized formula of the tunnel splitting energy (see Sec. III). In Sec. IV, we obtain the relaxation time by exactly diagonalizing the master equation. In Sec. V, solving the master equation analytically, we identify the dominant transition paths (see Figs. 9 and 10) and show that the magnetization reversal is not dominated by just one single path but rather by several paths which can be of comparable weight. We finally note that some of the results of the present paper have been published in Ref. 23 in a short and less general form. Here we present details of the derivation of these results and generalize them in various ways, leading to results such as satellite peaks in the overall relaxation curve, relaxation time of an individual relaxation path, an analytical expression for the effective linewidths, and a generalized tunnel splitting formula.

II. MODEL

In accordance with earlier work[12,14,17–19,24] we use a single-spin Hamiltonian $\mathcal{H}=\mathcal{H}_a+\mathcal{H}_Z+\mathcal{H}_{sp}+\mathcal{H}_T$ including spin-phonon coupling. This model turns out to be sufficient to describe the behavior of the Mn_{12}-acetate molecule (for temperatures $T\gtrsim 1$ K). In particular,

$$\mathcal{H}_a=-AS_z^2-BS_z^4 \tag{1}$$

represents the magnetic anisotropy where $A\gg B>0$. The anisotropy $-AS_z^2$ is depicted in Fig. 1. We define the easy axis to lie along the z direction.

Here, $\mathbf{S}$ is the spin operator with $s=10$, and $A/k_B=0.52-0.56$ K,[21,22] and $B/k_B=(1.1-1.3)\times 10^{-3}$ (Refs. 21 and 22) are the anisotropy constants (k_B is the Boltzmann factor). The Zeeman term

$$\mathcal{H}_Z=g\mu_B H_z S_z \tag{2}$$

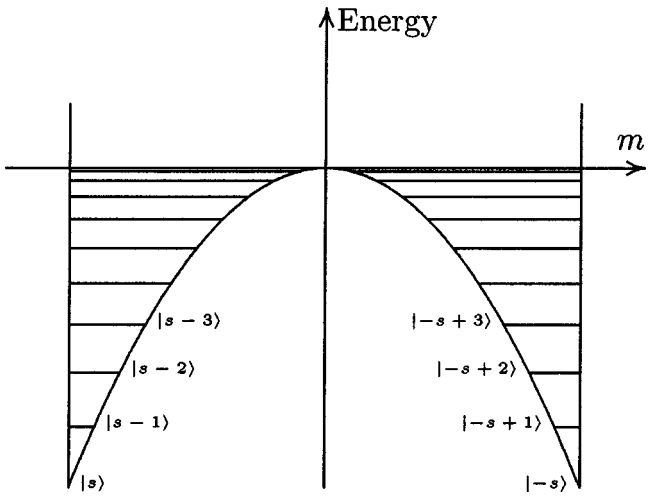

FIG. 1. Anisotropy energy $-Am^2-Bm^4$.

describes the coupling between the external magnetic field H_z and the spin $\mathbf{S}$. The g factor is known to be $g=1.9$.[25]

We denote by $|m\rangle$, $-s\leqslant m\leqslant s$, the eigenstates of $\mathcal{H}_a+\mathcal{H}_Z$ with eigenvalue

$$\varepsilon_m=-Am^2-Bm^4+g\mu_B H_z m. \tag{3}$$

If the external magnetic field H_z is increased, one obtains doubly degenerate spin states whenever a level m coincides with a level m' on the opposite side of the well (separated by the barrier given by A). The resonance condition for double degeneracy, i.e., $\varepsilon_m=\varepsilon_{m'}$, leads to the resonance field

$$H_z^{mm'}=\frac{n}{g\mu_B}[A+B(m^2+m'^2)]. \tag{4}$$

As usual, we refer to $n=m+m'=$ even (odd) as even (odd) resonances.

The Hamiltonian

$$\mathcal{H}_T=-\frac{1}{2}B_4(S_+^4+S_-^4)+g\mu_B H_x S_x, \tag{5}$$

makes tunneling between S_z states possible, where $S_\pm=S_x\pm iS_y$, and B_4 is the fourth-order anisotropy constant. $H_x=|\mathbf{H}|\sin\theta$ is the transverse field, with θ being the misalignment angle. H_x is assumed to be much smaller than H_z, i.e., θ is at most a few degrees. From experiments[21] it is known that $B_4/k_B=(4.3-14.4)\times 10^{-5}$ K. Finally, the most general spin-phonon coupling[26] which is allowed by the tetragonal symmetry of the Mn_{12} crystal in leading order is given by

$$\begin{aligned}\mathcal{H}_{sp}=&g_1(\epsilon_{xx}-\epsilon_{yy})\otimes(S_x^2-S_y^2)+\frac{1}{2}g_2\epsilon_{xy}\otimes\{S_x,S_y\}\\&+\frac{1}{2}g_3(\epsilon_{xz}\otimes\{S_x,S_z\}+\epsilon_{yz}\otimes\{S_y,S_z\})\\&+\frac{1}{2}g_4(\omega_{xz}\otimes\{S_x,S_z\}+\omega_{yz}\otimes\{S_y,S_z\}),\end{aligned} \tag{6}$$

$$=\frac{1}{2}g_1(\epsilon_{xx}-\epsilon_{yy})\otimes(S_+^2+S_-^2)+\frac{i}{4}g_2\epsilon_{xy}\otimes(S_-^2-S_+^2)$$
$$+\frac{1}{4}g_3[(\epsilon_{xz}-i\epsilon_{yz})\otimes\{S_+,S_z\}+(\epsilon_{xz}+i\epsilon_{yz})\otimes\{S_-,S_z\}]$$
$$+\frac{1}{4}g_4[(\omega_{xz}-i\omega_{yz})\otimes\{S_+,S_z\}+(\omega_{xz}+i\omega_{yz})\otimes\{S_-,S_z\}], \tag{7}$$

where g_i, $i=1,2,3,4$, are the spin-phonon coupling constants, which we shall determine in the following.

The linear strain tensor is defined by $\epsilon=\nabla\mathbf{u}$, where $\mathbf{u}(x,y,z)$ is the displacement field. Symmetrization of the strain tensor yields

$$\epsilon_{\alpha\beta}=\frac{1}{2}\left(\frac{\partial u_\alpha}{\partial\beta}+\frac{\partial u_\beta}{\partial\alpha}\right), \tag{8}$$

while the antisymmetrized linear strain tensor reads

$$\omega_{\alpha\beta}=\frac{1}{2}\left(\frac{\partial u_\alpha}{\partial\beta}-\frac{\partial u_\beta}{\partial\alpha}\right), \tag{9}$$

with $\alpha,\beta=x,y,z$. To determine g_i occurring in Eq. (6) we follow Dohm and Fulde.[27] The displacement

$$\mathbf{u}=\delta\boldsymbol{\phi}\times\mathbf{x} \tag{10}$$

(in leading order) is generated by rotation only. The infinitesimal rotation angle can be calculated by acting with $\boldsymbol{\nabla}_\mathbf{x}$ (with respect to the position $\mathbf{x}$) on both sides of Eq. (10),

$$\delta\boldsymbol{\phi}=\frac{1}{2}\boldsymbol{\nabla}\times\mathbf{u}=\begin{bmatrix}\omega_{yz}\\ \omega_{zx}\\ \omega_{xy}\end{bmatrix}. \tag{11}$$

Applying infinitesimal rotations on the spin vector $\mathbf{S}$

$$\begin{bmatrix}1&0&0\\0&1&\omega_{yz}\\0&-\omega_{yz}&1\end{bmatrix}\begin{bmatrix}1&0&\omega_{xz}\\0&1&0\\-\omega_{xz}&0&1\end{bmatrix}\begin{bmatrix}S_x\\S_y\\S_z\end{bmatrix}$$
$$=\begin{bmatrix}S_x+\omega_{xz}S_z\\S_y-\omega_{xz}\omega_{yz}S_x+\omega_{yz}S_z\\\omega_{xz}S_x-\omega_{yz}S_y-S_z\end{bmatrix}, \tag{12}$$

we find (to leading order in $\omega_{\alpha\beta}$) that the easy axis term, $-AS_z^2$, is transformed into

$$A(\omega_{xz}\{S_x,S_z\}+\omega_{yz}\{S_y,S_z\}). \tag{13}$$

Comparison with the last term in Eq. (6) then yields $g_4=2A$.

If the rotation matrices R_α, $\alpha=x,y,z$, are expanded up to second order, one finds terms that include symmetric elements of the strain tensor ϵ,

$$R_x=\begin{bmatrix}1&0&0\\0&1-\frac{1}{2}\delta\phi_x^2&-\delta\phi_x\\0&\delta\phi_x&1-\frac{1}{2}\delta\phi_x^2\end{bmatrix}, \tag{14}$$

$$R_y=\begin{bmatrix}1-\frac{1}{2}\delta\phi_y^2&0&-\delta\phi_y\\0&1&0\\\delta\phi_y&0&1-\frac{1}{2}\delta\phi_y^2\end{bmatrix}, \tag{15}$$

$$R_z=\begin{bmatrix}1-\frac{1}{2}\delta\phi_z^2&-\delta\phi_z&0\\\delta\phi_z&1-\frac{1}{2}\delta\phi_z^2&0\\0&0&1\end{bmatrix}. \tag{16}$$

Now we obtain from $\mathbf{u}=R_zR_yR_x\mathbf{x}-\mathbf{x}$

$$\mathbf{u}=\delta\boldsymbol{\phi}\times\mathbf{x}-\frac{1}{2}\begin{bmatrix}(\delta\phi_y^2+\delta\phi_z^2)x\\(\delta\phi_x^2+\delta\phi_z^2)y\\(\delta\phi_x^2+\delta\phi_y^2)z\end{bmatrix}. \tag{17}$$

By keeping derivatives of $\delta\phi_\alpha$, up to second order we find $\delta\phi_x^2=\epsilon_{xx}-\epsilon_{yy}-\epsilon_{zz}$, and cyclic permutation of (x,y,z).

After inserting the rotated spin vector $R_xR_y\mathbf{S}$ into $-AS_z^2=-A(\mathbf{S}^2-S_x^2-S_y^2)$ we get for the right-hand side

$$A(\epsilon_{xx}-\epsilon_{yy})(S_x^2-S_y^2)+O(\epsilon^2), \tag{18}$$

where we retain only terms that induce spin transitions. Comparing with the spin-phonon Hamiltonian (6) one sees immediately that $g_1=A$, and thus

$$g_1=g_4/2=A. \tag{19}$$

Thus the coupling constants g_1 and g_4 are explicitly expressed in terms of the anisotropy A.

Finally, we note that the terms in Eq. (6) that are proportional to $g_{1,2}$ produce second-order transitions with $\Delta m=\pm2$, while the ones proportional to $g_{3,4}$ produce first-order transitions with $\Delta m=\pm1$. Thus, Eq. (19) implies that first-order and second-order transitions are equally important for the relaxation. In following Abragam and Bleaney,[28] it is now very plausible to adopt the approximations $|g_2|\approx g_1=A$ and $|g_3|\approx g_4=2A$ (the sign is irrelevant for the transition rates calculated below).

III. MASTER EQUATION INCLUDING SPIN TUNNELING

A. Generalized master equation

In this section we derive a master equation that describes the relaxation of the spin due to phonon-assisted transitions including resonances due to tunneling. For this we make use of a standard formalism[29,30] suitable to describe a system (spin) coupled to a heat bath reservoir (phonons), the latter of which is in thermodynamic equilibrium described by the canonical density matrix $\rho_{\rm ph}$ for free phonons. That means we

start from the full Hamiltonian $\mathcal{H}=\mathcal{H}_0+\mathcal{H}_{\rm ph}+\mathcal{H}_{\rm sp}$, where $\mathcal{H}_0=\mathcal{H}_{\rm a}+\mathcal{H}_{\rm Z}+\mathcal{H}_{\rm T}$ represents the system, $\mathcal{H}_{\rm ph}$ the phonon heat bath, and $\mathcal{H}_{\rm sp}$ given in Eq. (6) is of the form $\mathcal{H}_{\rm sp}=\Sigma_i Q_i\otimes F_i$, where Q_i is a spin operator and F_i is a phonon operator. The generalized master equation in the interaction picture (I) in Born and Markoff approximation reads [see Eq. (8.1.22) in Ref. 29]

$$\dot{\rho}^I(t)=-\left(\frac{1}{\hbar}\right)^2\sum_{ij}\int_0^\infty dt''\{[Q_i(t),Q_j(t-t'')\rho^I(t)]\times\langle F_i(t'')F_j\rangle-[Q_i(t),\rho^I(t)Q_j(t-t'')]\langle F_jF_i(t'')\rangle\}, \tag{20}$$

where $Q_i(t)=e^{i\mathcal{H}_0t}Q_ie^{-i\mathcal{H}_0t}$. Equation (20) is valid for the situations where the correlation time τ_c in the heat bath is much smaller than the relaxation time τ of the spin system. Indeed, the assumption is satisfied here since a rough estimate for thermal phonons yields $\tau_c\sim\hbar/k_BT\sim10^{-11}$ s, at $T=1$ K, whereas it will turn out that $\tau\gtrsim1$ s (see below). In this case, the integral kernel gives a vanishing contribution for times t'' larger than τ_c, and thus one can extend the upper limit of the time integral to infinity and replace $\rho(t-t'')$ by $\rho(t)$ (see also Ref. 30, Chap. 13).

As our undamped Hamiltonian $\mathcal{H}_0$ has also nondiagonal elements in the $|m\rangle$ basis it proves convenient to formulate the generalized master equation in the Schrödinger picture, i.e., with $\rho^I(t)=e^{(i/\hbar)\mathcal{H}_0t}\rho(t)e^{-(i/\hbar)\mathcal{H}_0t}$, we get

$$\dot{\rho}(t)=\frac{i}{\hbar}[\rho(t),\mathcal{H}_0]-\left(\frac{1}{\hbar}\right)^2\sum_{ij}\int_0^\infty dt''\{[Q_i,Q_j(-t'')\rho(t)]\times\langle F_i(t'')F_j\rangle-[Q_i,\rho(t)Q_j(-t'')]\langle F_jF_i(t'')\rangle\}. \tag{21}$$

As the tunnel splitting generated by $\mathcal{H}_{\rm T}$ is smaller than the level spacing of $\mathcal{H}_0$, i.e., $E_{mm'}<|\varepsilon_m-\varepsilon_{m'}|$ (see below), we can approximate the free propagator $e^{-(i/\hbar)\mathcal{H}_0t''}$ within the integral kernel by $e^{-(i/\hbar)(\mathcal{H}_{\rm a}+\mathcal{H}_{\rm Z})t''}$ in the rest of our calculations.[31] Next, we take the matrix elements of Eq. (21) using $\rho_{mm'}=\langle m|\rho|m'\rangle$, $\rho_m=\rho_{mm}$, $\mathcal{U}_{mm'}=e^{-(i/\hbar)(\varepsilon_m-\varepsilon_{m'})t''}$, and with the definitions[29,32]

$$\Gamma^+_{mkln}=\frac{1}{\hbar^2}\sum_{i,j}\langle m|Q_i|k\rangle\langle l|Q_j|n\rangle\int_0^\infty dt''\mathcal{U}_{ln}\langle F_i(t'')F_j\rangle,$$

$$\Gamma^-_{mkln}=\frac{1}{\hbar^2}\sum_{i,j}\langle m|Q_i|k\rangle\langle l|Q_j|n\rangle\int_0^\infty dt''\mathcal{U}_{mk}\langle F_jF_i(t'')\rangle,$$

$$\gamma_{m'm}=\sum_k(\Gamma^+_{m'kkm'}+\Gamma^-_{mkkm})-\Gamma^+_{mmm'm'}-\Gamma^-_{mmm'm'},$$

$$W_{mn}=\Gamma^+_{nmmn}+\Gamma^-_{nmmn}, \tag{22}$$

it follows from Eq. (21) that

$$\dot{\rho}_{mm'}=\frac{i}{\hbar}[\rho,\mathcal{H}_0]_{mm'}+\delta_{mm'}\sum_{n\neq m}\rho_nW_{mn}-\gamma_{mm'}\rho_{mm'}, \tag{23}$$

where we have considered only the secular terms [i.e., the ''coarse-grained'' derivative was taken with respect to t in Eq. (20)][29] and set $[,]_{mm'}=\langle m|[,]|m'\rangle$. The relaxation of the magnetization is entirely based on Eq. (23).

The difference to the usual master equation is that Eq. (23) takes also off-diagonal elements of the density matrix $\rho(t)$ into account. This is essential to describe tunneling of the magnetization, which is caused by the overlap of the S_z states.

The diagonal elements ($m=m'$) of Eq. (23) yield the master equation

$$\dot{\rho}_m=\frac{i}{\hbar}[\rho,\mathcal{H}_0]_{mm}+\sum_{n\neq m}\rho_nW_{mn}-\rho_m\sum_{n\neq m}W_{nm}. \tag{24}$$

The equation for the off-diagonal elements ($m\neq m'$),

$$\dot{\rho}_{mm'}=\frac{i}{\hbar}[\rho,\mathcal{H}_0]_{mm'}-\gamma_{mm'}\rho_{mm'}, \tag{25}$$

can be simplified in the following way. According to Eq. (7), Q_i is an element of the set $\{S_+^2,S_-^2,S_+S_z,S_zS_+,S_-S_z,S_zS_-\}$. Hence, we see that $\Gamma^+_{mmm'm'}=\Gamma^-_{mmm'm'}=0$, and we get

$$\gamma_{m'm}=\gamma_{mm'}=\frac{1}{2}\sum_n(W_{nm'}+W_{nm})=\frac{1}{2}(W_m+W_{m'}), \tag{26}$$

where we use the abbreviation $W_m=\Sigma_nW_{nm}$.

Evaluation of Eq. (22) leads immediately to Fermi's golden rule for transition rates in first quantization [see Eq. (8.2.3) in Ref. 29]:

$$W_{mn}=\frac{2\pi}{\hbar}\sum_{NN'}|\langle mN|H_{\rm sp}|nN'\rangle|^2\langle N'|\rho_{\rm ph}|N'\rangle\delta(E_{N'}-E_N-\varepsilon_m+\varepsilon_n). \tag{27}$$

Explicit evaluation yields (see Appendix A)

$$W_{m\pm1,m}=\frac{A^2s_{\pm1}}{12\pi\rho c^5\hbar^4}\frac{(\varepsilon_{m\pm1}-\varepsilon_m)^3}{e^{\beta(\varepsilon_{m\pm1}-\varepsilon_m)}-1},$$

$$W_{m\pm2,m}=\frac{17A^2s_{\pm2}}{192\pi\rho c^5\hbar^4}\frac{(\varepsilon_{m\pm2}-\varepsilon_m)^3}{e^{\beta(\varepsilon_{m\pm2}-\varepsilon_m)}-1}, \tag{28}$$

where $s_{\pm1}=(s\mp m)(s\pm m+1)(2m\pm1)^2$, and $s_{\pm2}=(s\mp m)(s\pm m+1)(s\mp m-1)(s\pm m+2)$. The mass density ρ for Mn_{12} is given by 1.83×10^3 kg/m^3.[33] Here, c is the sound velocity of the Mn crystal, which is the only free parameter in our theory. As already mentioned, we are not aware of direct measurements of c (but see below). Note that the transition rates $W_{m\pm1,m}, W_{m\pm2,m}$ are very sensitive to variations of the sound velocity c, as the latter enters with the fifth power.

B. Spin tunneling

We include now the spin tunneling in the generalized master equation (23). Let $|m\rangle$ and $|m'\rangle$ be two eigenstates of $\mathcal{H}_{\rm a}+\mathcal{H}_{\rm Z}$ on the left and right sides of the barrier, respectively. $|m\rangle$ and $|m'\rangle$ are degenerate when $\delta H_z=H_z^{mm'}-H_z$ vanishes. In the presence of tunneling, induced by $\mathcal{H}_{\rm T}$, the

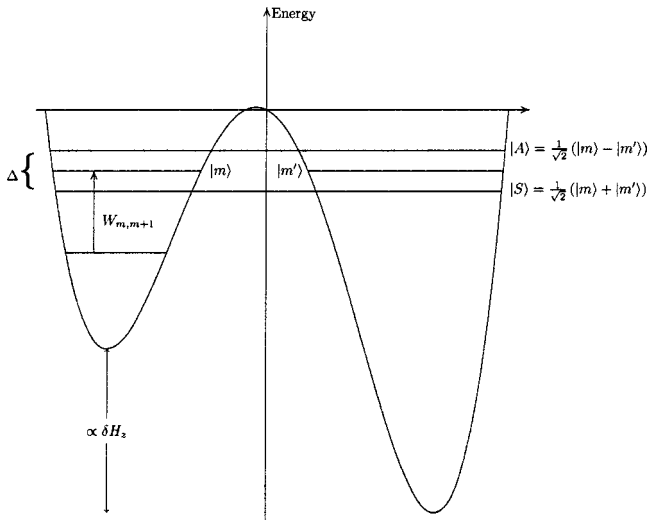

FIG. 2. Tunneling configuration.

two states form (anti)symmetric levels split by $E_{mm'}$ (for $\delta H_z = 0$). By using time-independent perturbation theory in higher order the tunnel splitting energy $E_{mm'}$ can be evaluated,[34]

$$E_{mm'} = 2\frac{V_{m,m-1}}{\varepsilon_{m-1}-\varepsilon_m}\frac{V_{m-1,m-2}}{\varepsilon_{m-2}-\varepsilon_m}\cdots V_{-m'+1,-m'}. \quad (29)$$

Note that in this expression only steps with $\Delta m = \pm 1$ are allowed. However, for the present purpose we need to generalize Eq. (29) to situations where potentials $V_{m_i,m_{i+1}} \in \mathbb{R}$ with arbitrary steps $\Delta m = m_i - m_{i+1}$ $(m > m_i > m_{i+1} > m'$, $i = 1, \ldots, N-1)$ can occur. As we will show in Appendix B this is indeed possible by using resolvent techniques, and we find

$$E_{mm'} = 2\left|\sum_{\substack{m_1,\ldots,m_N \\ m_i \neq m,m'}} \frac{V_{m,m_1}}{\varepsilon_m - \varepsilon_{m_1}} \prod_{i=1}^{N-1} \frac{V_{m_i,m_{i+1}}}{\varepsilon_m - \varepsilon_{m_{i+1}}} V_{m_N,m'}\right|, \quad (30)$$

where N is the lowest order of the degenerate perturbation theory, by means of which Eq. (30) has been derived (Nth-order secular equation[35]), giving a nonvanishing contribution to $E_{mm'}$. For the potentials $V_{m_i,m_{i+1}}$ we insert combinations of terms occurring in $\mathcal{H}_T$. For example, the anisotropy B_4 leads to transitions $\Delta m = \pm 4$, while the misalignment H_x leads to transitions $\Delta m = \pm 1$. The summations in Eq. (30) can be thought of as summation over different paths in the Hilbert space connecting $|m\rangle$ with $|m'\rangle$.

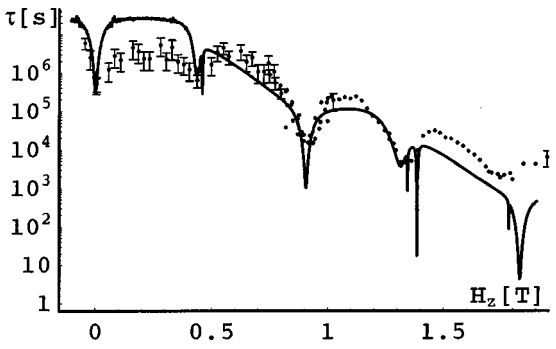

FIG. 3. Full line: semilogarithmic plot of calculated relaxation time τ as function of magnetic field H_z at $T = 1.9$ K. The optimal fit values (see text) are $A/k_B = 0.54$ K, $B/k_B = 1.1\times10^{-3}$ K, and $B_4/k_B = 8.5\times10^{-5}$ K, $\theta = 1°$, and $c = 1.45\times10^3$ m/s. Dots and error bars: data taken from Ref. 7.

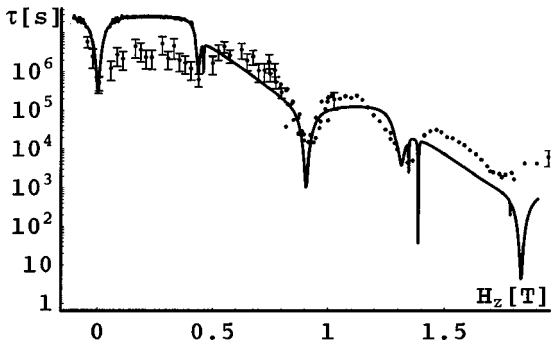

FIG. 4. Full line: semilogarithmic plot of calculated relaxation time τ as function of magnetic field H_z at $T = 1.9$ K. Here $\theta = 0.5°$ has been chosen. Dots and error bars: data taken from Ref. 7.

Continuing the evaluation of the first part of Eq. (23) we project the undamped Hamiltonian $\mathcal{H}_0$ by $P = \Sigma_{n=m,m'}|n\rangle\langle n|$ on the two-state system $\{|m\rangle, |m'\rangle\}$, which yields the two-state Hamiltonian in the presence of a bias field (see Fig. 2)

$$\overline{\mathcal{H}_T} = \xi_m|m\rangle\langle m| + \frac{E_{mm'}}{2}|m\rangle\langle m'| + (m \leftrightarrow m')$$

$$\hat{=} \begin{bmatrix} \xi_m & \frac{E_{mm'}}{2} \\ \frac{E_{mm'}}{2} & \xi_{m'} \end{bmatrix} = P\mathcal{H}_0 P, \quad (31)$$

with $\xi_m = \varepsilon_m + g\mu_B \delta H_z m$ and the energy eigenvalues $E_T = \frac{1}{2}[\xi_m + \xi_{m'} \pm \sqrt{(\xi_m - \xi_{m'})^2 + E_{mm'}^2}]$. $\overline{\mathcal{H}_T}$ provides a valid description as long as the level splitting remains smaller than the level spacing, i.e.,

$$\Delta = \sqrt{(\xi_m - \xi_{m'})^2 + E_{mm'}^2} \ll |\varepsilon_{m^{(\prime)}} - \varepsilon_{m^{(\prime)}\pm 1}|. \quad (32)$$

We have checked that between two main resonances this condition is satisfied for the states $|m_T\rangle$ and $|m'_T\rangle$ of the

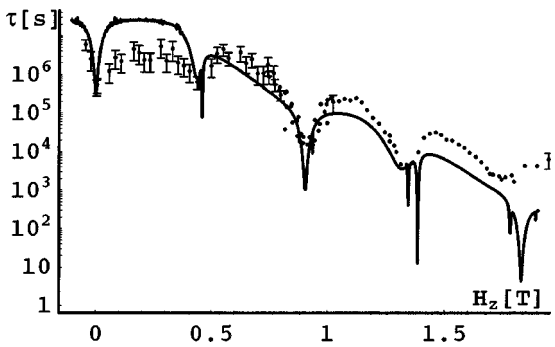

FIG. 5. Full line: semilogarithmic plot of calculated relaxation time τ as function of magnetic field H_z at $T = 1.9$ K. Here $\theta = 2°$ has been chosen. Dots and error bars: data taken from Ref. 7.

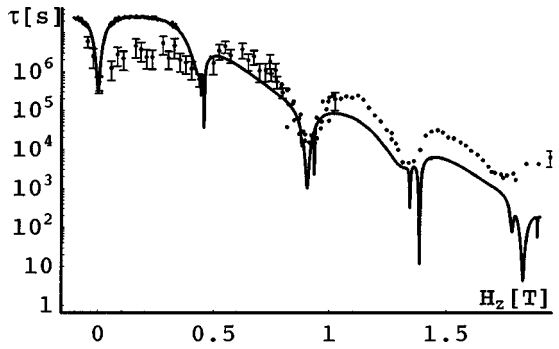

FIG. 6. Full line: semilogarithmic plot of calculated relaxation time τ as function of magnetic field H_z at $T=1.9$ K. Here $\theta=3°$ has been chosen. Dots and error bars: data taken from Ref. 7.

dominant paths and for each degenerate pair of states $|m\rangle$, $|m'\rangle$ with $\varepsilon_m,\varepsilon_{m'}\leqslant\varepsilon_{m_T},\varepsilon_{m'_T}$ (see Sec. V).

Next we insert the two-state Hamiltonian $\overline{\mathcal{H}}_T$ into the generalized master equation (23), which yields

$$\dot{\rho}_m=\frac{iE_{mm'}}{2\hbar}(\rho_{mm'}-\rho_{m'm})-W_m\rho_m+\sum_{n\neq m,m'}W_{mn}\rho_n \tag{33}$$

and

$$\dot{\rho}_{mm'}=-\left(\frac{i}{\hbar}\xi_{mm'}+\gamma_{mm'}\right)\rho_{mm'}+\frac{iE_{mm'}}{2\hbar}(\rho_m-\rho_{m'}), \tag{34}$$

where $\xi_{mm'}=\xi_m-\xi_{m'}$, and likewise for $m\leftrightarrow m'$. Ultimately, we are interested in the overall relaxation time τ of the quantity $\rho_s-\rho_{-s}$ (see Sec. V) due to phonon-induced transitions. This τ turns out to be much longer than $\tau_d=1/\gamma_{mm'}$, which is the decoherence time of the decay of the off-diagonal elements $\rho_{mm'}\propto e^{-t/\tau_d}$ of the density matrix ρ. Thus, we can neglect the time-dependence of the off-diagonal elements, i.e., $\dot{\rho}_{mm'}\approx 0$. Physically this means that we deal with incoherent tunneling for times $t>\tau_d$.[36] Inserting then the stationary solution of Eq. (34) into Eq. (33), which leads to the complete master equation including resonant as well as nonresonant levels,

$$\dot{\rho}_m=-W_m\rho_m+\sum_{n\neq m,m'}W_{mn}\rho_n+\Gamma_m^{m'}(\rho_{m'}-\rho_m), \tag{35}$$

where

$$\Gamma_m^{m'}=E_{mm'}^2\frac{W_m+W_{m'}}{4\xi_{mm'}^2+\hbar^2(W_m+W_{m'})^2} \tag{36}$$

is the transition rate from m to m' (induced by tunneling) in the presence of phonon damping.[38] The relaxation dynamics of the resonances described by $1/\Gamma_m^{m'}\sim 10^{-7}$ s (see Fig. 15) turns out to be much faster than the phonon-induced overall relaxation, i.e., $1/\Gamma_m^{m'}\ll\tau\gtrsim 1$s (see Fig. 3). Thus, our derivation based on the assumption $\tau\gg\tau_d$ is self-consistent since $1/\Gamma_m^{m'}\sim\tau_d$. Note that Eq. (35) is now of the usual form of a master equation, i.e., only diagonal elements of the density matrix $\rho(t)$ occur. For levels $k\neq m,m'$, Eq. (35) reduces to

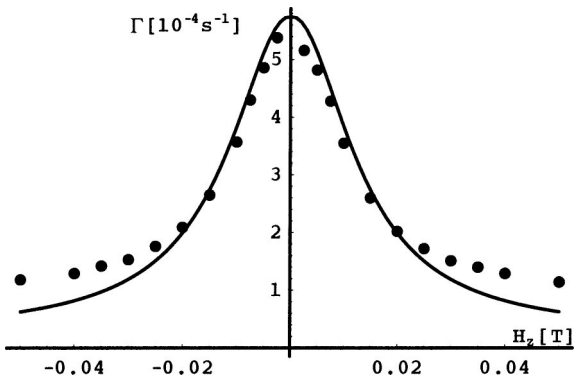

FIG. 7. Full line: plot of calculated relaxation rate $\Gamma=1/\tau$ as function of H_z for the first resonance peak at $T=2.6$ K. The Lorentzian shape is due to $\Gamma_m^{m'}$ in Eq. (36). The optimal fit values (see text) are $A/k_B=0.56$ K, $B/k_B=1.3\times10^{-3}$ K, and $B_4/k_B=14.4\times10^{-5}$ K, $\theta=1°$, and $c=2.0\times10^3$ m/s. Dots: data taken from Ref. 11.

$$\dot{\rho}_k=-W_k\rho_k+\sum_n W_{kn}\rho_n. \tag{37}$$

We note that $\Gamma_m^{m'}$ has a Lorentzian shape with respect to the external magnetic field δH_z occurring in $\xi_{mm'}$. The H_z dependence of W_m around the resonances turns out to be much weaker (see below) and can be safely ignored. It is thus this $\Gamma_m^{m'}$ that will determine the peak shape of the magnetization resonances (see below and Figs. 3–8). Note that in Figs. 3–8 these Lorentzians are *truncated* at the center of the peak by the spin-phonon transition rates W_m and $W_{m'}$ in such a way that the effective linewidth (defined as the width at half of the height of the truncated peak) is much larger than $(W_m+W_{m'})/2$. This needs some further explanations, which are given in Sec. VI, after we have discussed the relaxation times.

IV. RELAXATION TIME

A. Numerical diagonalization of the master equation

In this section we give the results of our exact evaluation obtained by a numerical diagonalization of the master equa-

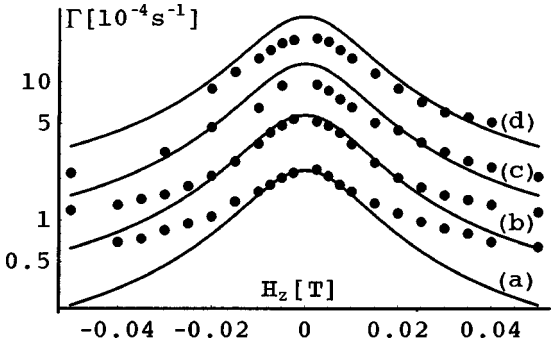

FIG. 8. Full lines: semilogarithmic plots of calculated relaxation rate $\Gamma=1/\tau$ as function of H_z for the first resonance peak at (a) $T=2.5$ K, (b) $T=2.6$ K, (c) $T=2.7$ K, and (d) $T=2.8$ K. All peaks are of single Lorentzian shape. The optimal fit values are the same as in Fig. 7. Dots: data taken from Ref. 11.

tion. For convenience we now write down the master equation (35) as a vector equation,

$$\dot{\vec{\rho}}(t)=\tilde{W}\vec{\rho}(t), \tag{38}$$

where the elements of the vector $\vec{\rho}(t)$ are the diagonal elements of the density matrix ρ. Within the interval I_{n_1,n_2} [see Eq. (65)] delimited by the two main resonances n_1 and n_2 only the tunneling rates $\Gamma_{m_1}^{m_1'}$ and $\Gamma_{m_2}^{m_2'}$ [Eq. (36)], for which $m_1+m_1'=n_1$ and $m_2+m_2'=n_2$ (see Sec. V A) are allowed to be included for self-consistency reasons: the tunnel splitting (32) entering Γ is only valid within this interval I_{n_1,n_2}. If w_i, $i=1,2,\ldots,21$, are the eigenvalues of the rate matrix $\tilde{W}$, the dominant relaxation time of the spin system is given by

$$\tau=\max_i\left\{-\frac{1}{\mathrm{Re}\, w_i}\right\}. \tag{39}$$

The eigenvalues w_i turn out to be nondegenerate with the smallest one being far separated by a factor of at least 10^4 from the remaining ones. The result is plotted in Fig. 3, where the overall relaxation rate τ is shown as a function of H_z at $T=1.9$ K. It is important to note that all the resonance peaks are of Lorentzian shape. We note that in our model the even resonances are induced by the quartic B_4 anisotropy, whereas the odd resonances are induced by product combinations of $B_4S_\pm^4$ and H_xS_x terms [see Eq. (30)]. For the plot in Fig. 3 we set $\theta=1°$ in accordance with the experimental uncertainty,[11] leading to a maximal transversal field H_x of about 350 G.

B. Comparison with experimental data

For comparison we also include in Fig. 3 the data reported by Thomas *et al.*[7,39] We have optimized the fit (as explained in the Introduction) in such a way that the fits of the model parameters, given by

$$A/k_B=0.54\ \text{K}, \tag{40}$$

$$B/k_B=1.1\times10^{-3}\ \text{K}, \tag{41}$$

$$B_4/k_B=8.5\times10^{-5}\ \text{K}, \tag{42}$$

are roughly within the reported experimental uncertainties of Refs. 21 and 22 (see above). The value of B_4 is in excellent agreement with recent measurements performed in Ref. 40. Our fit of the sound velocity yields

$$c=1.45\times10^3\ \text{m/s}. \tag{43}$$

There is a difference between odd and even resonances, i.e., the relaxation time τ at an even resonance peak is about three times smaller than the one at a subsequent odd resonance peak. It should be mentioned that almost identical plots are obtained for $0.5°\lesssim\theta\lesssim3°$, as can be seen in Figs. 3–6. The present theory holds for $|H_x|\lesssim1000$ G (which is well satisfied here); otherwise the shift of the levels $|m\rangle$ due to the perturbation H_xS_x must be taken into account. For example, for the resonance $n=3$ the relevant tunneling takes place between $|4\rangle$ and $|-1\rangle$. The dominant second-order shift

$$\begin{aligned}&\frac{\langle1|g\mu_BH_xS_x|0\rangle\langle0|g\mu_BH_xS_x|1\rangle}{\varepsilon_1-\varepsilon_0}\\&\quad+\frac{\langle1|g\mu_BH_xS_x|2\rangle\langle2|g\mu_BH_xS_x|1\rangle}{\varepsilon_1-\varepsilon_2}\\&=k_B\times40\ \text{mK}\\&\ll|\varepsilon_1|=k_B\times2.3\ \text{K}\end{aligned} \tag{44}$$

clearly shows that the unperturbed states $\{|m\rangle\}$ are a good zeroth-order approximation. It is also important to know whether the second-order shifts caused by the perturbation $\mathcal{H}_\mathrm{T}$ are negligible compared to the tunnel splitting $E_{m_\mathrm{T}m_\mathrm{T}'}$. Explicitly, we find

$$\begin{aligned}|\Delta_2^{(2)}-\Delta_{-6}^{(2)}|/k_B&=8.5\ \text{mK}\quad(n=4),\\|\Delta_1^{(2)}-\Delta_{-4}^{(2)}|/k_B&=13.2\ \text{mK}\quad(n=3),\\|\Delta_3^{(2)}-\Delta_{-5}^{(2)}|/k_B&=5.0\ \text{mK}\quad(n=2),\\|\Delta_2^{(2)}-\Delta_{-3}^{(2)}|/k_B&=0.5\ \text{mK}\quad(n=1),\\|\Delta_4^{(2)}-\Delta_{-4}^{(2)}|/k_B&=0\quad(n=0),\end{aligned} \tag{45}$$

where $\Delta_{m_\mathrm{T}}^{(2)}$ is the second-order shift of the unperturbed states $|m_\mathrm{T}\rangle$ of the dominant paths. These renormalizations cause a very small shift of the resonance peaks, e.g., the shift for $n=3$ is 0.6 mT. The relevant tunnel splitting energies of the odd and even resonances are about the same (except $E_{4,-1}$):

$$\begin{aligned}E_{4,-4}&\approx E_{3,-2}\approx E_{5,-3}\approx k_B\times45\ \text{mK},\\E_{4,-1}/k_B&\approx130\ \text{mK},\quad E_{6,-2}/k_B\approx40\ \text{mK}.\end{aligned} \tag{46}$$

For comparison, $E_{2,-2}/k_B\approx1$ K [see also Eq. (66)]. In conclusion, the diagonal elements of the shifts of the nondegenerate perturbation theory are much smaller than the off-diagonal elements of the shifts of the degenerate perturbation theory (see Appendix B). Thus our assumption of quasidegeneracy is very well satisfied.

We note that there are satellite peaks in Figs. 3–6, the origin of which will be explained below in Sec. V.

In Figs. 7 and 8 we plot the peaks of the first resonance at $H_z=0$, which is induced only by the B_4 anisotropy, for four different temperatures, namely $T=2.5$, 2.6, 2.7, and 2.8 K. The four peaks (like all others) are of single Lorentzian shape as a result of the two-state transition rate $\Gamma_m^{m'}$ given in Eq. (36). For comparison we plot in Figs. 7 and 8 the data reported by Friedman *et al.*[11] for the same temperatures (no error bars, however, are given in Ref. 11). The optimal fit values are

$$A/k_B=0.56\ \text{K}, \tag{47}$$

$$B/k_B=1.3\times10^{-3}\ \text{K}, \tag{48}$$

$$B_4/k_B=14.4\times10^{-5}\ \text{K}, \tag{49}$$

$$c=2.0\times10^3\ \text{m/s}. \tag{50}$$

Note that these values are the same for all four temperatures, which means that our peaks fit also the temperature dependence of the relaxation time. The fitting parameters turn out to be somewhat larger than the ones used in Fig. 3 [see Eqs. (40)–(42)], which could be caused by sample differences, e.g., in volume-to-surface ratio and/or in shape anisotropy of the samples, etc. Indeed, the sample of Ref. 11 consists of many small crystallites in contrast to the single crystal used by Thomas *et al.*[7] In any case, the differences are small, and the sound velocity c seems to be within the expected order of magnitude. Clearly, it would be highly desirable to check this prediction by an independent and direct measurement of c. On the other hand,[41] we can get an independent estimate for c from the specific heat and the Debye temperature Θ_D which was recently measured in Mn_{12}.[42] The reported value is $\Theta_D=(38\pm4)$ K, and making use of the Debye relation[43]

$$k_B\Theta_D=\hbar\omega_D=\hbar c k_D, \quad \text{with } n=\frac{k_D^3}{6\pi^2}=\frac{1}{V_0}, \tag{51}$$

we find

$$c=(1.77-2.18)\times10^3 \text{ m/s}, \tag{52}$$

where ω_D is the Debye frequency, k_D the Debye wave vector, and $V_0=3716$ Å^3 the unit-cell volume. Comparing this value for c with the one obtained before, see Eqs. (43) and (50), we see that the agreement is very good. This result corroborates not only our prediction of c but also our values obtained for the spin-phonon coupling constants g_i.

Finally we also mention that the prefactor $A^2 s_{\pm1}/12\pi\rho c^5\hbar^4$ of our spin-phonon rates [Eq. (28)] is in excellent agreement with the value of the parameter denoted by C in a recent paper.[44] Note that their fit of the parameter[44] C is not as precise as ours, because C is assumed to be independent of the spin states $\{|m\rangle\}$.

To summarize our results obtained so far, we see that the agreement between theory and experiment is satisfactory; in particular we emphasize that there is no free fit parameter. Thus, our model and its evaluation seems to contain the essential physics responsible for the magnetization relaxation in Mn_{12}.

C. Comparison with previous results

In comparison to previous results we obtain much better agreement between theory and experiment for the following reasons. For this comparison we can restrict ourselves to the work of Fort *et al.*,[18] since — as far as we are aware of — it has produced the best agreement with the relaxation data[7] thus far. First, the spin-phonon coupling constants g_1, g_2, and g_3 are explicitly given in our work (g_4 has been found before[14]). As shown in Sec. II we find them to be of order $A=0.56$ K, and it is this value which leads to good agreement with all known experimental data which involve these coupling constants.[6,7,44] In contrast, Fort *et al.*[18] set arbitrarily the g_i's to values of 15 K and 30 K, which is clearly in contradiction to our microscopic values. Moreover, our value for the fit parameter B_4 fulfills the constraints of independent measurements,[13,16,21,22] while Fort *et al.*[18] obtain a B_4 value which is about 30 times smaller than the measured value in Ref. 21. From Figs. 7 and 8 we see that the temperature dependence of the relaxation time agrees quite well with the measurements of Friedman *et al.*[11]

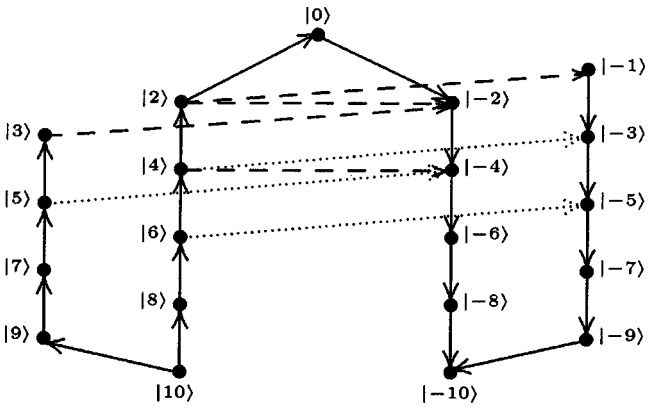

FIG. 9. Spin relaxation paths (from $m=10$ to $m=-10$) for $0\leqslant g\mu_B H_z\leqslant A+13B$. Full lines: thermal transitions due to phonons. Dashed lines: dominant tunneling transitions due to B_4 and H_x terms. Dotted lines: tunneling transitions that lead to satellite peaks [included in the numerical diagonalization of the master equation (38)]. The states where paths intersect are denoted as vertices.

V. RELAXATION PATHS

A. Analytical result

In order to get a better physical understanding for the relaxation process of the spin system it is instructive to determine the dominant transition paths via which the spin can relax into its ground state. For this we derive an approximate analytic expression for the relaxation time denoted by τ^* (to distinguish it from the exact τ obtained in the previous section). First, we solve the master equation for one *particular* transition path n which does not intersect with other paths. For $H_z\geqslant0$ we find (derivation is given below)

$$\tau_n=\frac{1}{1+e^{\beta(\varepsilon_{-s}-\varepsilon_s)}}\sum_{\{m_i\}_n}\frac{e^{\beta(\varepsilon_{m_i}-\varepsilon_s)}}{\Omega_{m_i}^{m_{i+1}}}, \tag{53}$$

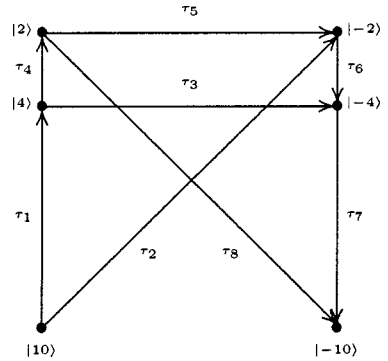

FIG. 10. Serially reduced diagram associated with Fig. 9. In order to understand the analytical evaluation of the relaxation diagram in Fig. 9 better, tunneling transitions that lead to satellite peaks are excluded. The relaxation times τ_n are given in Eq. (53). For $|H_z|\lesssim0.05$ T only the path $\tau_1\rightarrow\tau_3\rightarrow\tau_7$ is dominant (see Figs. 7 and 8).

where $\Omega_{m_i}^{m_{i+1}}=\Omega_{m_i\to m_{i+1}}=W_{m_{i+1}m_i}$ or $\Gamma_{m_{i+1}}^{m_i}$, depending on the particular path n characterized by the sum over the levels m (see Figs. 9 and 10). Equation (53) holds for arbitrary initial (ε_i) and final (ε_f) energies, and for arbitrary steps $\Delta m=m_{i+1}-m_i$ (see below).

We now turn to the derivation of the relaxation time of a cascade including the external field H_z. For this we need to go beyond the results obtained previously[17] for $H_z=0$, which requires a non-trivial extension. We start with rewriting the master equation (35) as

$$\dot\rho_s=\Omega_{m_1}^{s}\rho_{m_1}-\Omega_{s}^{m_1}\rho_s,$$

$$\dot\rho_{m_j}=\Omega_{m_{j+1}}^{m_j}\rho_{m_{j+1}}+\Omega_{m_{j-1}}^{m_j}\rho_{m_{j-1}}-\Omega_{m_j}^{m_{j+1}}\rho_{m_j}-\Omega_{m_j}^{m_{j-1}}\rho_{m_j},$$

$$\dot\rho_{-s}=\Omega_{m_p}^{-s}\rho_{m_p}-\Omega_{-s}^{m_p}\rho_{-s}, \tag{54}$$

with $m_j\in]-s,s[$, $m_j>m_{j+1}$, $j=1,\ldots,p\leqslant 2s-1$, and $\dot\rho_{m_j}=d\rho_{m_j}/dt$. We consider now the stationary limit of Eq. (54) which we define by

$$\dot\rho_s=-J,\quad \dot\rho_{m_j}=0,\quad \dot\rho_{-s}=J, \tag{55}$$

where the first and last equation express conservation of the probability current J, which we assume positive for $H_z\geqslant 0$ and independent of m. Equation (55) leads to $p+1$ equations,

$$J(t)=\Omega_{m_i}^{m_{i+1}}\rho_{m_i}-\Omega_{m_{i+1}}^{m_i}\rho_{m_{i+1}}, \tag{56}$$

and by solving for $\rho_{m_{i+1}}$ we get

$$\rho_{m_i}=\frac{\Omega_{m_{i+1}}^{m_i}}{\Omega_{m_i}^{m_{i+1}}}\rho_{m_{i+1}}+\frac{J}{\Omega_{m_i}^{m_{i+1}}}, \tag{57}$$

where we have introduced $i=0,\ldots,p\leqslant 2s-1$, and $m_0=s$. To simplify the following treatment we assume detailed balance also for the tunneling processes. This approximation has little effect on the final result which turns out to agree very well with the exact relaxation time τ where no such approximations are invoked. Inserting then the detailed balance relation $\Omega_{m_{i+1}}^{m_i}/\Omega_{m_i}^{m_{i+1}}=e^{\beta(\varepsilon_{m_{i+1}}-\varepsilon_{m_i})}$ one obtains

$$\rho_{m_i}=e^{\beta(\varepsilon_{m_{i+1}}-\varepsilon_{m_i})}\rho_{m_{i+1}}+\frac{J}{\Omega_{m_i}^{m_{i+1}}}. \tag{58}$$

In order to get an equation that depends on ρ_{-s} and ρ_s only one has to sum over the following $p+1$ equations:

$$\rho_s=e^{\beta(\varepsilon_{m_1}-\varepsilon_s)}\rho_{m_1}+\frac{J}{\Omega_s^{m_1}},$$

$$e^{\beta(\varepsilon_{m_1}-\varepsilon_s)}\rho_{m_1}=e^{\beta(\varepsilon_{m_2}-\varepsilon_s)}\rho_{m_2}+\frac{Je^{\beta(\varepsilon_{m_1}-\varepsilon_s)}}{\Omega_{m_1}^{m_2}},$$

$$e^{\beta(\varepsilon_{m_2}-\varepsilon_s)}\rho_{m_2}=e^{\beta(\varepsilon_{m_3}-\varepsilon_s)}\rho_{m_3}+\frac{Je^{\beta(\varepsilon_{m_2}-\varepsilon_s)}}{\Omega_{m_2}^{m_3}},$$

$$\vdots$$

$$e^{\beta(\varepsilon_{m_p}-\varepsilon_{-s})}\rho_{m_p}=e^{\beta(\varepsilon_{-s}-\varepsilon_s)}\rho_{-s}+\frac{Je^{\beta(\varepsilon_{m_p}-\varepsilon_s)}}{\Omega_{m_p}^{-s}},$$

$$\rho_s=e^{\beta(\varepsilon_{-s}-\varepsilon_s)}\rho_{-s}+J\sum_{m_i}\frac{e^{\beta(\varepsilon_{m_i}-\varepsilon_s)}}{\Omega_{m_i}^{m_{i+1}}}. \tag{59}$$

In the special case of $H_z=0$, i.e., $\varepsilon_s-\varepsilon_{-s}=0$, Eq. (59) agrees with previous results.[14]

Taking the time derivative of Eq. (59) and using $\dot\rho_{-s}/\dot\rho_s=-1$ we find

$$\dot\rho_{\pm s}=\pm\frac{\dot J}{1+e^{\beta(\varepsilon_{-s}-\varepsilon_s)}}\sum_{m_i}\frac{e^{\beta(\varepsilon_{m_i}-\varepsilon_s)}}{\Omega_{m_i}^{m_{i+1}}}, \tag{60}$$

and thus

$$\dot\rho_s-\dot\rho_{-s}=2\frac{\dot J}{1+e^{\beta(\varepsilon_{-s}-\varepsilon_s)}}\sum_{m_i}\frac{e^{\beta(\varepsilon_{m_i}-\varepsilon_s)}}{\Omega_{m_i}^{m_{i+1}}}=-2J. \tag{61}$$

The solution of the last differential equation is

$$J(t)=J_0e^{-t/\tau^*}, \tag{62}$$

with the relaxation time

$$\tau^*=\frac{1}{1+e^{\beta(\varepsilon_{-s}-\varepsilon_s)}}\sum_{m_i}\frac{e^{\beta(\varepsilon_{m_i}-\varepsilon_s)}}{\Omega_{m_i}^{m_{i+1}}},\quad H_z\geqslant 0. \tag{63}$$

Finally, the summation $\Sigma_{\{m_i\}_n}$ in Eq. (53) is defined as the summation Σ_{m_i} in Eq. (63) taken only from m_{initial} to $m_{\text{final}}+1$, where $|m_{\text{initial}}\rangle,|m_{\text{final}}\rangle$ denote any two neighboring vertices (where paths intersect) in Figs. 9, 16, 18, and 20 (see below).

Similarly one can solve the rate equations (55) for $J<0\Leftrightarrow H_z\leqslant 0$. Then we obtain

$$\tau^*=\frac{1}{1+e^{\beta(\varepsilon_s-\varepsilon_{-s})}}\sum_{m_i}\frac{e^{\beta(\varepsilon_{m_i}-\varepsilon_{-s})}}{\Omega_{m_{i+1}}^{m_i}},\quad H_z\leqslant 0, \tag{64}$$

which for $H_z=0$ (i.e., $\varepsilon_{-s}=\varepsilon_s$) and steps $\Delta m=\pm 1$ reduces to the result found in Ref. 14.

If there is more than one path contributing to the relaxation (which is typically the case in the region between two resonances), we have to account for intersections at vertices. For this we associate with each path a probability current $J_n=\dot\rho_n$, and interpret Eq. (53) in terms of a serial circuit with the summands playing the role of ''resistances.'' This allows us then to set up flow diagrams for J_n (see Figs. 9, 10, and 16–21), which obey the analog of Kirchhoff's rules:

(K1) $\Sigma_n J_n=0$: The sum over all incoming and outgoing currents vanishes at a vertex (current conservation).

(K2) $\Sigma_n J_n \tau_n = \Delta N$: The sum over all voltage drops $(J_n \tau_n)$ is equal to the source-drain voltage $\Delta N = \rho_s - \rho_{-s}$ for any closed path (probability conservation).

The total probability current is given by $J = \Delta \dot{N}$. For every interval

$$I_{n_1,n_2} = [H_z^{m_{\mathrm{T},1} m'_{\mathrm{T},1}}, H_z^{m_{\mathrm{T},2} m'_{\mathrm{T},2}}] \tag{65}$$

[see Eq. (4)], where $n_1 = m_{\mathrm{T},1} + m'_{\mathrm{T},1}$, $n_2 = m_{\mathrm{T},2} + m'_{\mathrm{T},2}$, $0 \leqslant n_1 = n_2 + 1 \leqslant 3$, a set of equations is given by the rules (K1) and (K2). For every set we derive the relaxation time $\tau^*_{n_1,n_2} = \Delta N / J$.

Figure 9 shows the complete, Fig. 10 its serially reduced flow diagram for $0 \leqslant H_z \leqslant (1/g\mu_B)(A + 13B)$. From (K1) we get

$$J = J_1 + J_2, \quad J_2 + J_5 = J_6,$$

$$J_1 = J_3 + J_4, \quad J_3 + J_6 = J_7,$$

$$J_4 = J_5 + J_8, \quad J_7 + J_8 = J,$$

while from (K2) we get

$$\Delta N = J_1 \tau_1 + J_3 \tau_3 + J_7 \tau_7,$$

$$J_3 \tau_3 = J_4 \tau_4 + J_5 \tau_5 + J_6 \tau_6,$$

$$J_2 \tau_2 = J_1 \tau_1 + J_4 \tau_4 + J_5 \tau_5,$$

$$J_8 \tau_8 = J_5 \tau_5 + J_6 \tau_6 + J_7 \tau_7.$$

From these equations we obtain

$$\begin{aligned}
\tau^*_{0,1}(H_z) = (&\tau_4\tau_1\tau_5\tau_2 + \tau_8\tau_4\tau_1\tau_2 + \tau_8\tau_1\tau_5\tau_2 + \tau_8\tau_4\tau_1\tau_6 + \tau_4\tau_7\tau_5\tau_2 + \tau_4\tau_7\tau_2\tau_6 + \tau_8\tau_7\tau_5\tau_6 + \tau_8\tau_7\tau_2\tau_4 + \tau_4\tau_7\tau_5\tau_6 \\
&+ \tau_8\tau_7\tau_2\tau_3 + \tau_4\tau_7\tau_2\tau_3 + \tau_8\tau_4\tau_3\tau_7 + \tau_8\tau_3\tau_5\tau_7 + \tau_4\tau_3\tau_5\tau_7 + \tau_8\tau_3\tau_2\tau_6 + \tau_8\tau_4\tau_3\tau_2 + \tau_4\tau_3\tau_2\tau_6 + \tau_8\tau_4\tau_3\tau_6 \\
&+ \tau_8\tau_3\tau_5\tau_2 + \tau_8\tau_3\tau_5\tau_6 + \tau_8\tau_7\tau_5\tau_2 + \tau_8\tau_1\tau_2\tau_6 + \tau_8\tau_1\tau_5\tau_6 + \tau_3\tau_1\tau_5\tau_6 + \tau_8\tau_3\tau_1\tau_6 + \tau_7\tau_1\tau_5\tau_2 + \tau_3\tau_1\tau_2\tau_6 \\
&+ \tau_3\tau_1\tau_5\tau_7 + \tau_7\tau_1\tau_2\tau_6 + \tau_7\tau_1\tau_5\tau_6 + \tau_7\tau_1\tau_2\tau_4 + \tau_8\tau_6\tau_1\tau_7 + \tau_4\tau_1\tau_5\tau_7 + \tau_8\tau_4\tau_1\tau_7 + \tau_8\tau_3\tau_1\tau_2 + \tau_7\tau_1\tau_2\tau_3 \\
&+ \tau_8\tau_3\tau_1\tau_7 + \tau_3\tau_1\tau_5\tau_2 + \tau_8\tau_1\tau_5\tau_7 + \tau_8\tau_7\tau_2\tau_6 + \tau_8\tau_4\tau_7\tau_6 + \tau_4\tau_3\tau_5\tau_6 + \tau_4\tau_3\tau_5\tau_2 + \tau_4\tau_1\tau_2\tau_6 \\
&+ \tau_4\tau_1\tau_5\tau_6)/(\tau_8\tau_5\tau_2 + \tau_8\tau_5\tau_6 + \tau_8\tau_3\tau_2 + \tau_8\tau_4\tau_3 + \tau_4\tau_5\tau_6 + \tau_8\tau_4\tau_6 + \tau_8\tau_4\tau_2 + \tau_4\tau_2\tau_6 + \tau_4\tau_7\tau_6 + \tau_8\tau_3\tau_5 \\
&+ \tau_7\tau_2\tau_6 + \tau_7\tau_5\tau_6 + \tau_7\tau_5\tau_2 + \tau_7\tau_2\tau_3 + \tau_4\tau_1\tau_5 + \tau_3\tau_1\tau_5 + \tau_8\tau_1\tau_5 + \tau_8\tau_3\tau_1 + \tau_3\tau_2\tau_6 + \tau_3\tau_5\tau_6 + \tau_3\tau_5\tau_2 + \tau_3\tau_5\tau_7 \\
&+ \tau_4\tau_3\tau_7 + \tau_4\tau_3\tau_5 + \tau_8\tau_6\tau_1 + \tau_3\tau_1\tau_7 + \tau_7\tau_1\tau_6 + \tau_4\tau_1\tau_6 + \tau_3\tau_1\tau_6 + \tau_4\tau_1\tau_7 + \tau_8\tau_4\tau_1 + \tau_8\tau_2\tau_6 + \tau_4\tau_5\tau_2 + \tau_4\tau_3\tau_6 \\
&+ \tau_2\tau_4\tau_7 + \tau_7\tau_1\tau_5).
\end{aligned}$$

When $\tau^*_{0,1}$ is plotted as function of H_z there is no visible difference between the exact τ obtained in Sec. IV and this approximate τ^*, which confirms that the diagram in Fig. 9 contains the physically relevant relaxation paths for the interval $I_{0,1}$. Similar results are obtained for the other intervals, whose diagrams and calculations are shown in Appendix C.

Finally, near a resonance [$|\delta H_z| < w'$, see Eq. (74)] the above expression for τ^*; Eq. (53), strongly simplifies since we find that there is only one dominant relaxation path which involves only one tunneling channel. This finally explains why the peak shape is given by a single Lorentzian. We call the five strongest broadened resonances in Figs. 3–6 the main resonances. For every main resonance n we have identified [using Eq. (53)] its dominant path and its associated tunneling channel between the states $|m_{\mathrm{T}}\rangle$ and $|m'_{\mathrm{T}}\rangle$. These states are

n	m_{T}	m'_{T}
0	4	−4
1	3	−2
2	5	−3
3	4	−1
4	6	−2

(66)

Our calculation of the intermediate relaxation times τ_n provides a further prediction which could be tested with NMR techniques of the type described in Ref. 44.

B. Satellite peaks

Beside the main resonances there are also other narrower resonances (see Figs. 3–6) that are a direct consequence of the fourth-order anisotropy constant B [see Eq. (1)]. Indeed,

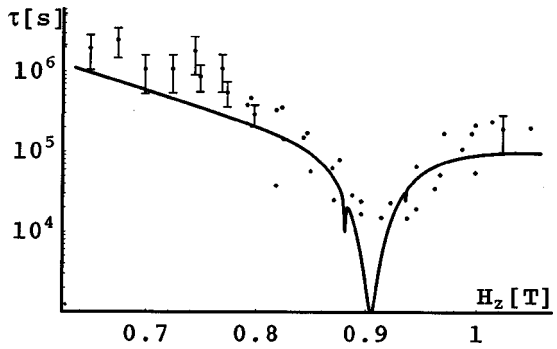

FIG. 11. Full line: semilogarithmic plot of calculated relaxation time τ as function of magnetic field H_z at $T=1.9$ K in the interval $3A/2g\mu_B \leqslant H_z \leqslant 5A/2g\mu_B$ with a higher resolution. The tunneling transition from $|5\rangle$ and $|-3\rangle$ is responsible for the main peak. Two satellite peaks are visible. The left (right) one is due to the tunneling channel between $|4\rangle$ and $|-2\rangle$ ($|6\rangle$ and $|-4\rangle$). Here $\theta=2°$ has been chosen. Dots and error bars: data taken from Ref. 7.

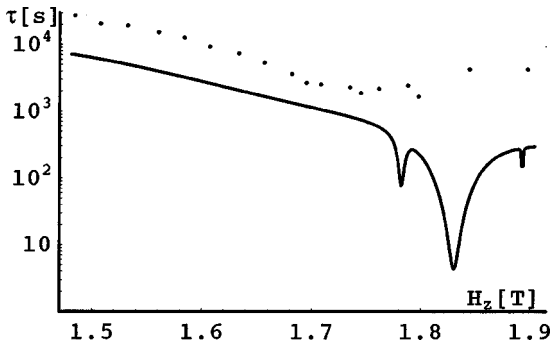

FIG. 13. Full line: semilogarithmic plot of calculated relaxation time τ as function of magnetic field H_z at $T=1.9$ K in the interval $7A/2g\mu_B \leqslant H_z \leqslant 9A/2g\mu_B$ with a higher resolution. The tunneling transition from $|6\rangle$ and $|-2\rangle$ is responsible for the main peak. Two satellite peaks are visible. The left (right) one is due to the tunneling channel between $|5\rangle$ and $|-1\rangle$ ($|7\rangle$ and $|-3\rangle$). Here $\theta=2°$ has been chosen. Dots and error bars: data taken from Ref. 7.

if the plots around one peak are magnified further, satellite peaks become visible (see Figs. 11–14). In order to understand the occurrence of these satellite peaks it is instructive to look at Fig. 18 below. There are several paths which can be used in the relaxation process. As we include the fourth-order anisotropy term, $-BS_z^4$, the resonance condition is not the same for every level [see Eq. (4)]. Hence, very narrow peaks show up, which can be seen only at high resolution. In Fig. 18 several additional tunneling paths, some of which are responsible for the satellite peaks in Figs. 11 and 12, have to be drawn (represented by the dotted lines in Fig. 18). For example, the tunnel splitting energy of the path from $|4\rangle$ to $|-2\rangle$ is proportional to $H_x B_4 H_x$ (third-order perturbation), where the ordering of the factors corresponds to the chosen path. Due to the presence of H_x^2 the width of the satellite peak (see next section) depends on the misalignment angle θ. If one takes a close look at our high resolution plots this difference between Fig. 11 and Fig. 12 is observable. It must be noted that we consider only tunnel splitting energies up to second order in B_4 and third order in H_x (also combinations such as $B_4^2 H_x^3$) for all the main and satellite peaks. Narrower satellite peaks are neglected.[45] The distance $d^{m_2 m_2'}_{m_1 m_1'}$ between a satellite peak and its associated main peak caused by a main resonance is given by Eq. (4),

$$d^{m_2 m_2'}_{m_1 m_1'} = |H_z^{m_1 m_1'} - H_z^{m_2 m_2'}| = \left| \frac{nB}{g\mu_B} (m_1^2 + m_1'^2 - m_2^2 - m_2'^2) \right|, \tag{67}$$

where m_1, m_1' (m_2, m_2') are responsible for the satellite (main) peak, and $n = m_1 + m_1' = m_2 + m_2'$. It would be interesting to search experimentally for these satellite peaks, which requires a higher experimental resolution of the peaks than achieved so far.

VI. WIDTH OF THE LORENTZIANS

In this section we give a physical interpretation of the effective half-width of the Lorentzian peaks in our plots. In order to get an expression for the width of our main and satellite peaks consider a Lorentzian $\Gamma(H_z)$ with linewidth w (see Fig. 15). If the upper part of this Lorentzian is cut off (where the curve is already very narrow) and both ends are connected by a horizontal line one obtains a curve that still has the same single Lorentzian shape for all practical purposes but now with an effective linewidth $w' > w$. Changing the tunnel matrix element $E_{mm'}$ results in a different truncation of the Lorentzian, thus changing the effective linewidth w'. We shall now estimate the effective linewidth w' and compare it with the one obtained from the exact $1/\tau$. Taking only the largest terms of Eq. (53) gives a rough approxima-

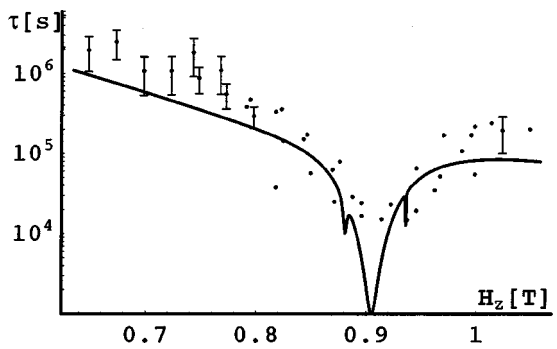

FIG. 12. Same plot as in Fig. 11, but with a misalignment angle of $\theta=3°$. Dots and error bars: data taken from Ref. 7.

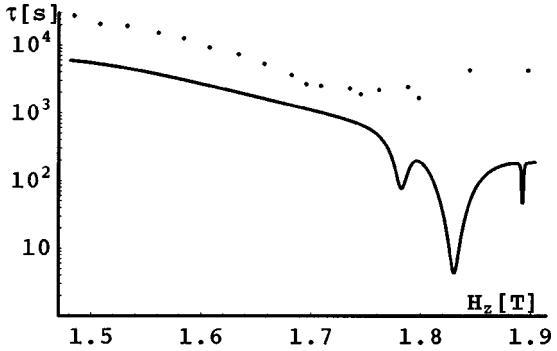

FIG. 14. Same plot as in Fig. 13, but with a misalignment angle of $\theta=3°$. Dots and error bars: data taken from Ref. 7.

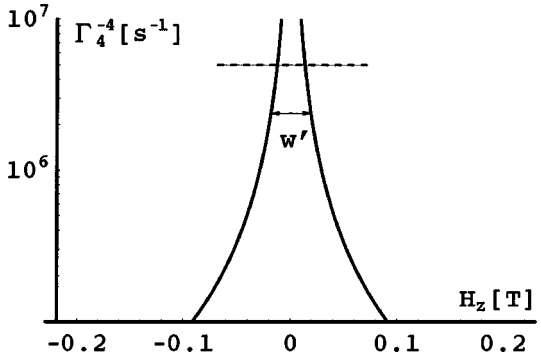

FIG. 15. Truncated Lorentzian Γ_4^{-4} with $A/k_B=0.56$ K, $B/k_B=1.3\times10^{-3}$ K, and $B_4/k_B=14.4\times10^{-5}$ K, $\theta=1°$, and $c=2.0\times10^3$ m/s, $w'=37.4$ mT (w' agrees very well with the width of the Lorentzian in Fig. 7), and $\Gamma_4^{-4}(w'/2)=2.4\times10^6$ s^{-1}. The truncation is indicated by the dashed line.

tion of the relaxation time near a resonance where the states $|m\rangle$ and $|m'\rangle$ are degenerate,

$$\tau'=\frac{1}{1+e^{\beta(\varepsilon_{-s}-\varepsilon_s)}}\left(\frac{e^{\beta(\varepsilon_{m+2}-\varepsilon_s)}}{W_{m,m+2}}+\frac{e^{\beta(\varepsilon_{m'}-\varepsilon_s)}}{W_{m'-2,m'}}+\frac{e^{\beta(\varepsilon_m-\varepsilon_s)}}{\Gamma_m^{m'}}\right). \tag{68}$$

Using the detailed balance relation

$$\frac{W_{m,m+2}}{W_{m+2,m}}=e^{\beta(\varepsilon_{m+2}-\varepsilon_m)} \tag{69}$$

we obtain the following approximation:

$$\tau'=\frac{e^{\beta(\varepsilon_{m+2}-\varepsilon_s)}}{1+e^{\beta(\varepsilon_{-s}-\varepsilon_s)}}\left(\frac{2}{W_{m,m+2}}+\frac{1}{\Gamma_m^{m'}}\right), \tag{70}$$

where we assumed that $W_{m,m+2}\approx W_{m'-2,m'}$.[46] In the limit $\xi_{mm'}\to0$ the phonon-damped tunneling rate $\Gamma_m^{m'}$ is much larger than $W_{m,m+2}$, so

$$\lim_{\xi_{mm'}\to0}\tau'\approx\frac{2e^{\beta(\varepsilon_{m+2}-\varepsilon_s)}}{(1+e^{\beta(\varepsilon_{-s}-\varepsilon_s)})W_{m,m+2}}. \tag{71}$$

The half-width of $\tau'(H_z)$, denoted by w', is then determined by the condition $\tau'(w'/2)=\tau'(0)/2$. This condition is fulfilled when

$$\Gamma_m^{m'}=\frac{W_{m,m+2}}{2}. \tag{72}$$

Thus we obtain the expression for the effective linewidth w',

$$w'=\frac{2\sqrt{W_m+W_{m'}}}{|m-m'|g\mu_B}\left[\frac{E_{mm'}^2}{W_{m,m+2}}-\frac{\hbar^2(W_m+W_{m'})}{4}\right]^{1/2}. \tag{73}$$

Since the height $E_{mm'}^2/\hbar^2(W_m+W_{m'})$ of the Lorentzian $\Gamma_m^{m'}$ is very large compared to its linewidth $|m-m'|g\mu_B w/\hbar=(W_m+W_{m'})/2$ and $W_m+W_{m'}\approx2W_{m,m+2}$ for the dominant paths (see Sec. V) we get the following reasonably accurate approximation for the effective linewidths in our plots:

$$w'=\frac{2^{3/2}E_{mm'}}{|m-m'|g\mu_B}. \tag{74}$$

Comparison with our exact calculations of the relaxation time shows that w' of Eq. (74) gives a very good estimate for the effective linewidth of the peaks in our plots (see Figs. 3–8 and 11–15).

VII. CONCLUSION

We have presented a comprehensive theoretical description of spin relaxation due to phonon-induced transitions and tunnel resonances. Deriving a generalized master equation (in Born and Markoff approximation) we obtain an exact numerical evaluation of the overall relaxation time τ as function of the longitudinal magnetic field H_z comprising Lorentzian-shaped peaks. In order to perform this evaluation we calculate the phonon-assisted transition rates of the spins, the spin-phonon coupling constants, and the tunnel splitting energy, for which a generalized formula is derived. The fourth-order diagonal terms in the Hamiltonian give rise to satellite peaks, the experimental observation of which requires a higher resolution of $\tau(H_z)$ than achieved so far. Our approximate analytical solution of the master equation yields a clear physical understanding of the relaxation process by revealing the relaxation paths that are followed by the spin. This solution provides the prediction of all involved intermediate relaxation times τ_n, which can be tested experimentally. The results of our model calculation agree well with *all* known data. We have been able to get agreement between theory and the entire relaxation curve. In addition, we have obtained reasonable agreement between theory and four single resonance peaks recently measured to high accuracy at four different temperatures. The formalism presented in this work has been applied to the specific parameter values of Mn_{12}, but many results derived here are generally valid and can be used for similar spin systems as well.

ACKNOWLEDGMENTS

We are grateful to H. Schoeller and T. Pohjola for useful comments. This work has been supported by the Swiss National Science Foundation.

APPENDIX A: SPIN-PHONON RATES

In order to evaluate the spin-phonon rates W_{mn} of Eq. (27) we first change to the Fourier representation. If $\mathbf{q}$ is a phonon wave vector, we can write $\mathbf{u}(\mathbf{x})$ as follows:

$$\mathbf{u}(\mathbf{x})=\frac{1}{\sqrt{N}}\sum_{\mathbf{q}}\mathbf{u}(\mathbf{q})e^{i\mathbf{q}\cdot\mathbf{x}}, \tag{A1}$$

with N being the number of unit cells. Hence

$$\boldsymbol{\epsilon}(\mathbf{x})=\frac{i}{\sqrt{N}}\sum_{\mathbf{q}}\begin{bmatrix}q_xu_x(\mathbf{q}) & q_xu_y(\mathbf{q}) & q_xu_z(\mathbf{q})\\ q_yu_x(\mathbf{q}) & q_yu_y(\mathbf{q}) & q_yu_z(\mathbf{q})\\ q_zu_x(\mathbf{q}) & q_zu_y(\mathbf{q}) & q_zu_z(\mathbf{q})\end{bmatrix}e^{i\mathbf{q}\cdot\mathbf{x}}. \tag{A2}$$

After (anti)symmetrization, these matrix elements can be inserted into the expression (7),

$$\mathcal{H}_{\rm sp}=\frac{1}{\sqrt{N}}\sum_{j,\mathbf{q}} i\Big\{\frac{1}{2}g_1[q_x u_x(\mathbf{q})-q_y u_y(\mathbf{q})]\otimes(S_+^2+S_-^2)$$
$$+\frac{i}{8}g_2[q_x u_y(\mathbf{q})+q_y u_x(\mathbf{q})]\otimes(S_-^2-S_+^2)$$
$$+\frac{1}{8}g_3[q_x u_z(\mathbf{q})+q_z u_x(\mathbf{q})-i(q_y u_z(\mathbf{q})+q_z u_y(\mathbf{q}))]$$
$$\otimes\{S_+,S_z\}+\frac{1}{8}g_3[q_x u_z(\mathbf{q})+q_z u_x(\mathbf{q})+i(q_y u_z(\mathbf{q})$$
$$+q_z u_y(\mathbf{q}))]\otimes\{S_-,S_z\}+\frac{1}{8}g_4[q_x u_z(\mathbf{q})+q_z u_x(\mathbf{q})$$
$$-i(q_y u_z(\mathbf{q})+q_z u_y(\mathbf{q}))]\otimes\{S_+,S_z\}+\frac{1}{8}g_4[q_x u_z(\mathbf{q})$$
$$-q_z u_x(\mathbf{q})+i(q_y u_z(\mathbf{q})-q_z u_y(\mathbf{q}))]\otimes\{S_-,S_z\}\Big\}e^{i\mathbf{q}\cdot\mathbf{R}_j}. \tag{A3}$$

$\mathbf{R}_j$ are the positions of the Mn_{12} molecules.

We proceed with the canonical transformation $(\mathbf{u},\mathbf{p})\rightarrow(\mathbf{c}^\dagger,\mathbf{c})$. $\mathbf{c}^{(\dagger)}=\boldsymbol{\epsilon}_{\mathbf{q}}c_{\mathbf{q}}^{(\dagger)}$ annihilates (creates) a phonon with wave vector $\mathbf{q}$ and polarization $\boldsymbol{\epsilon}_{\mathbf{q}}$, and

$$\mathbf{u}(\mathbf{q})=\sqrt{\frac{\hbar}{2M\omega_{\mathbf{q}}}}(\mathbf{c}^\dagger+\mathbf{c}), \tag{A4}$$

where M is the mass per unit cell. Inserting Eq. (A4) into Eq. (A3) and considering only the spin of the Mn_{12} molecule at $\mathbf{R}_j=0$ yields

$$\mathcal{H}_{\rm sp}=\sum_{\mathbf{q}} i\sqrt{\frac{\hbar}{2NM\omega_{\mathbf{q}}}}\Big\{\frac{1}{2}g_1[q_x(c_x^\dagger+c_x)-q_y(c_y^\dagger+c_y)]$$
$$\otimes(S_+^2+S_-^2)+\frac{i}{8}g_2[q_x(c_y^\dagger+c_y)+q_y(c_x^\dagger+c_x)]$$
$$\otimes(S_-^2-S_+^2)+\frac{1}{8}g_3[(q_x-iq_y)(c_z^\dagger+c_z)+q_z(c_x^\dagger+c_x$$
$$-ic_y^\dagger-ic_y)]\otimes\{S_+,S_z\}+\frac{1}{8}g_3[(q_x+iq_y)(c_z^\dagger+c_z)$$
$$+q_z(c_x^\dagger+c_x+ic_y^\dagger+ic_y)]\otimes\{S_-,S_z\}+\frac{1}{8}g_4[(q_x-iq_y)$$
$$\times(c_z^\dagger+c_z)-q_z(c_x^\dagger+c_x-ic_y^\dagger-ic_y)]\otimes\{S_+,S_z\}$$
$$+\frac{1}{8}g_4[(q_x+iq_y)(c_z^\dagger+c_z)-q_z(c_x^\dagger+c_x+ic_y^\dagger+ic_y)]$$
$$\otimes\{S_-,S_z\}\Big\}. \tag{A5}$$

This expression can be used to evaluate the transition probability. We employ the following standard relations:

$$c|n\rangle=\sqrt{n}|n-1\rangle,$$
$$c^\dagger|n\rangle=\sqrt{n+1}|n+1\rangle,$$
$$S_-|s,m\rangle=\sqrt{(s+m)(s-m+1)}|s,m-1\rangle,$$
$$S_+|s,m\rangle=\sqrt{(s-m)(s+m+1)}|s,m+1\rangle. \tag{A6}$$

The transition rate $W_{-2}=W_{m-2,m}$ [see Eq. (27)] for $m\rightarrow m-2$ $(\varepsilon_{m-2}\gtrless\varepsilon_m)$ can now be calculated in second quantization ($n_\alpha=n_{\mathbf{q},\alpha}$, $\alpha=x,y,z$ denotes the number of phonons with wave vector $\mathbf{q}$, polarization mode λ, and oscillation direction α, and the thermal average over phonons is left implicit),

$$W_{-2}=\frac{2\pi}{\hbar}\sum_{\mathbf{q}'}|\langle n_{\mathbf{q}'}\mp1,m-2|\mathcal{H}_{\rm sp}|n_{\mathbf{q}'},m\rangle|^2\delta'_\pm$$
$$=\sum_{\mathbf{q}}\frac{\pi}{NM\omega_{\mathbf{q}}}\Big[\frac{g_1^2}{4}(q_x\langle n_x\mp1|c_x^{(\dagger)}|n_x\rangle$$
$$-q_y\langle n_y\mp1|c_y^{(\dagger)}|n_y\rangle)^2|\langle m-2|S_-^2|m\rangle|^2$$
$$+\frac{g_2^2}{64}(q_x\langle n_y\mp1|c_y^{(\dagger)}|n_y\rangle+q_y\langle n_x\mp1|c_x^{(\dagger)}|n_x\rangle)^2$$
$$\times|\langle m-2|S_-^2|m\rangle|^2\Big]\delta_\pm$$
$$=\frac{1}{4}\sum_{\mathbf{q}}\frac{\pi s_{-2}}{NM\omega_{\mathbf{q}}}\begin{pmatrix}n_{\mathbf{q}}+1\\0\end{pmatrix}$$
$$\times\Big[g_1^2(q_x-q_y)^2+\frac{g_2^2}{16}(q_x+q_y)^2\Big]\delta_\pm, \tag{A7}$$

where $s_{-2}=(s+m)(s-m+1)(s+m-1)(s-m+2)$, and $\delta_\pm^{(\prime)}=\delta(\pm(\varepsilon_{m-2}-\varepsilon_m)-\hbar\omega_{\mathbf{q}^{(\prime)}})$.

With the approximation $g_1=A\approx g_2$ and the thermal average $\langle n_{\mathbf{q}}\rangle=1/(e^{\beta\hbar\omega_q}-1)$ one obtains

$$W_{-2}=\frac{1}{4}\sum_{\mathbf{q}}\frac{\pi A^2 s_{-2}}{NM\omega_q}\frac{(q_x-q_y)^2+\frac{1}{16}(q_x+q_y)^2}{\pm(e^{\pm\beta\hbar\omega_q}-1)}\delta_\pm. \tag{A8}$$

As a next step the sum is replaced by an integral $((1/N)\Sigma_{\mathbf{q}}\rightarrow[a^3/(2\pi)^3]\int d^3q)$ and the density $\rho=M/a^3$ is inserted,

$$W_{-2}=\frac{A^2 s_{-2}}{32\pi^2\rho}\int\frac{d^3q}{\omega_q}\frac{(q_x-q_y)^2+\frac{1}{16}(q_x+q_y)^2}{\pm(e^{\pm\beta\hbar\omega_q}-1)}\delta_\pm. \tag{A9}$$

After changing to spherical coordinates one gets

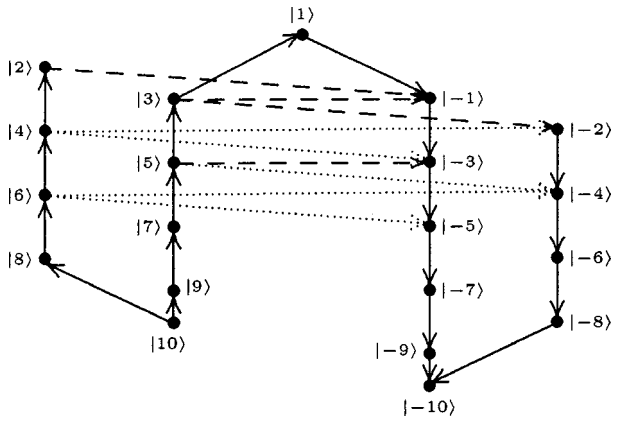

FIG. 16. Spin relaxation paths (from $m=10$ to $m=-10$) for $(1/g\mu_B)(A+13B)\leqslant H_z\leqslant(2/g\mu_B)(A+34B)$. Full lines: thermal transitions due to phonons. Dashed lines: dominant tunneling transitions due to B_4 and H_x terms. Dotted lines: tunneling transitions that lead to satellite peaks [included in the numerical diagonalization of the master equation (38)].

$$W_{-2}=\frac{17A^2s_{-2}}{192\pi\rho}\int_0^\infty\frac{dq}{\omega_q}\frac{q^4}{\pm(e^{\pm\beta\hbar\omega_q}-1)}\delta_\pm. \quad \text{(A10)}$$

Assuming a linear dispersion relation $\omega_q=cq$, where c is the sound velocity, and using $\varepsilon=\hbar\omega_q=\hbar cq$ one obtains

$$W_{-2}=\frac{17A^2s_{-2}}{192\pi\rho c^5\hbar^4}\int_0^\infty d\varepsilon\frac{\varepsilon^3}{\pm(e^{\pm\beta\hbar\omega_q}-1)}\delta_\pm$$

$$=\frac{17A^2s_{-2}}{192\pi\rho c^5\hbar^4}\frac{(\varepsilon_{m-2}-\varepsilon_m)^3}{e^{\beta(\varepsilon_{m-2}-\varepsilon_m)}-1}. \quad \text{(A11)}$$

In the same way we get

$$W_{+2}=\frac{17A^2s_{+2}}{192\pi\rho c^5\hbar^4}\frac{(\varepsilon_{m+2}-\varepsilon_m)^3}{e^{\beta(\varepsilon_{m+2}-\varepsilon_m)}-1}, \quad \text{(A12)}$$

with $s_{+2}=(s-m)(s+m+1)(s-m-1)(s+m+2)$.

The transition rates for $m\rightarrow m\pm1$ can be calculated in the same manner as above with $g_4=2A\approx g_3$,

$$W_{\pm1}=\frac{A^2s_{\pm1}}{12\pi\rho c^5\hbar^4}\frac{(\varepsilon_{m\pm1}-\varepsilon_m)^3}{e^{\beta(\varepsilon_{m\pm1}-\varepsilon_m)}-1}, \quad \text{(A13)}$$

where $s_{\pm1}=(s\mp m)(s\pm m+1)(2m\pm1)^2$, and $\rho=1.83\times10^3$ kg/m^3.[33]

APPENDIX B: LEVEL SPLITTING

In this appendix we derive a formula for the tunnel splitting energy which is applicable to potentials $V_{m_i,m_{i+1}}\in\mathbb{R}$ with arbitrary $\Delta m=m_i-m_{i+1}$ $(m>m_i>m_{i+1}>m'$, $i=1,\ldots,N-1)$. According to Kato's theory[47] the expansion of the resolvent

$$G(z)=\frac{1}{z-H_0-\lambda V} \quad \text{(B1)}$$

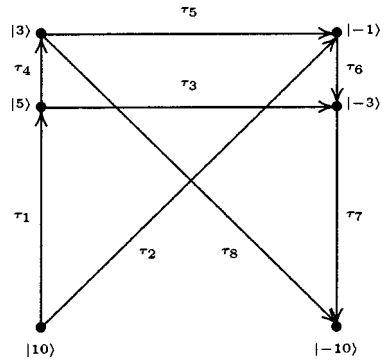

FIG. 17. Serially reduced diagram associated with Fig. 16. In order to understand the analytical evaluation of the relaxation diagram in Fig. 16 better, tunneling transitions that lead to satellite peaks are excluded. The relaxation times τ_n are given in Eq. (53).

leads to a rigorous treatment of the perturbation theory, which is very useful to evaluate high-order perturbation terms. We use the notation of Messiah.[47]

Let N be the order of the perturbation. Then the projection operator $P=\Sigma_m|m\rangle\langle m|$, consisting of the degenerate states $\{|m\rangle\}$, and the operator $(H-E_a^0)P$ are expanded as follows:

$$P=P_0+\sum_{N=1}^{\infty}\lambda^N A^{(N)}, \quad (H-E_a^0)P=\sum_{N=1}^{\infty}\lambda^N B^{(N)},$$

with

$$A^{(N)}=-\sum_{(N)}S^{k_1}VS^{k_2}V\cdots VS^{k_{N+1}},$$

$$B^{(N)}=-\sum_{(N-1)}S^{k_1}VS^{k_2}V\cdots VS^{k_{N+1}},$$

where

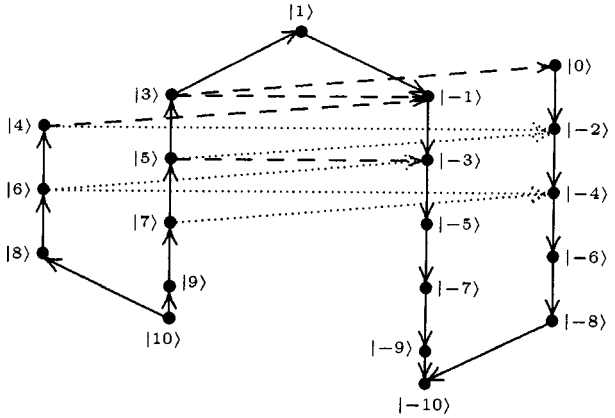

FIG. 18. Spin relaxation paths (from $m=10$ to $m=-10$) for $(2/g\mu_B)(A+34B)\leqslant H_z\leqslant(3/g\mu_B)(A+17B)$. Full lines: thermal transitions due to phonons. Dashed lines: dominant tunneling transitions due to B_4 and H_x terms. Dotted lines: tunneling transitions that lead to satellite peaks [included in the numerical diagonalization of the master equation (38)].

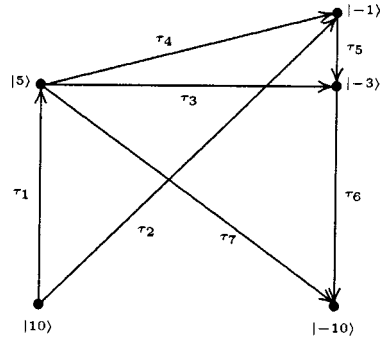

FIG. 19. Serially reduced diagram associated with Fig. 18. In order to understand the analytical evaluation of the relaxation diagram in Fig. 18 better, tunneling transitions that lead to satellite peaks are excluded. The relaxation times τ_n are given in Eq. (53).

$$S^k=\begin{cases} -P_0, & \text{if } k=0, \\ \dfrac{Q_0}{a^k}, & \text{if } k\geqslant 1, \end{cases}$$

$$Q_0=1-P_0, \quad \frac{Q_0}{a^k}=Q_0\frac{1}{(E_a^0-H_0)^k}Q_0,$$

and the sum $\Sigma_{(N)}$ has to be taken over all combinations $k_1,k_2,\cdots,k_{N+1}$ with the restriction $k_1+k_2+\ldots+k_{N+1}=N$.

The following general secular equation must be solved:

$$\det(H_a-\chi K_a)=\det(C_a)=0, \tag{B2}$$

where we have introduced the abbreviation $C_a=H_a-\chi K_a$. The χ are the eigenvalues of the perturbed states. H_a and K_a are defined by

$$H_a=P_0HPP_0=E_a^0K_a+P_0\sum_{N=1}^{\infty}\lambda^N B^{(N)}P_0, \tag{B3}$$

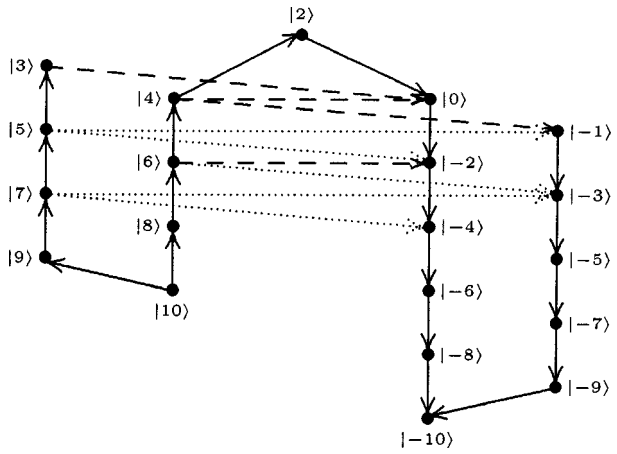

FIG. 20. Spin relaxation paths (from $m=10$ to $m=-10$) for $(3/g\mu_B)(A+17B)\leqslant H_z\leqslant(4/g\mu_B)(A+40B)$. Full lines: thermal transitions due to phonons. Dashed lines: dominant tunneling transitions due to B_4 and H_x terms. Dotted lines: tunneling transitions that lead to satellite peaks [included in the numerical diagonalization of the master equation (38)].

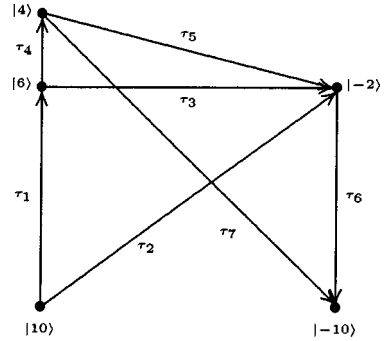

FIG. 21. Serially reduced diagram associated with Fig. 20. In order to understand the analytical evaluation of the relaxation diagram in Fig. 20 better, tunneling transitions that lead to satellite peaks are excluded. The relaxation times τ_n are given in Eq. (53).

$$K_a=P_0PP_0=P_0+P_0\sum_{N=1}^{\infty}\lambda^N A^{(N)}P_0. \tag{B4}$$

Thus we have now

$$C_a=(E_a^0-\chi)P_0+(E_a^0-\chi)\sum_{N=1}^{\infty}\lambda^N P_0A^{(N)}P_0 + \sum_{N=1}^{\infty}\lambda^N P_0B^{(N)}P_0. \tag{B5}$$

Equation (B5) is the general formula for finding the perturbed eigenvalues and eigenstates. We apply it now to the situation of our two degenerate spin states $|m\rangle$ and $|m'\rangle$. The following derivation refers to the off-diagonal elements of Eq. (B5).

The factors $P_0A^{(N)}P_0$ and $P_0B^{(N)}P_0$ do not vanish if $k_1=k_{N+1}=0$. As we look for the lowest-order perturbation that gives a contribution to the tunnel splitting $E_{mm'}$, the projection operators S^{k_i}, $i=2,\ldots,N$, must not be equal to $-P_0$, i.e., $k_i\neq 0$, $i=2,\ldots,N$. Hence, we get the following combinations for the lowest-order perturbation,

$$\text{for } A^{(N)}:\ k_2=k_3=\cdots=k_{i-1}=1, k_i=2, \quad k_{i+1}=\cdots=k_N=1, \quad i=2,\ldots,N, \tag{B6}$$

$$\text{for } B^{(N)}:\ k_2=k_3=\cdots=k_N=1. \tag{B7}$$

In the case of weak perturbation the second term of Eq. (B5) is much smaller than the third one. Thus the secular equation reads as follows:

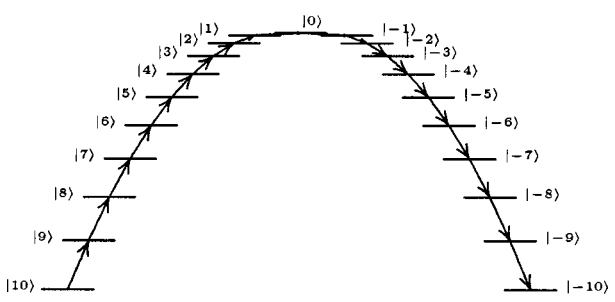

FIG. 22. Cascade with $\Delta m=-1$ and $\mathbf{H}=0$.

$$C_a=(E_a^0-\chi)P_0+(\text{diagonal elements})$$
$$+\sum_{N=1}^{\infty}\lambda^N\sum_{\substack{m_1,\ldots,m_N\\ m_i\neq m,m'}}|m\rangle\frac{V_{m,m_1}}{\varepsilon_m-\varepsilon_{m_1}}$$
$$\times\prod_{i=1}^{N-1}\frac{V_{m_i,m_{i+1}}}{\varepsilon_m-\varepsilon_{m_{i+1}}}V_{m_N,m'}\langle m'|. \tag{B8}$$

Thus we arrive at formula (30).

APPENDIX C: APPLICATION OF KIRCHHOFF'S RULES

In this appendix we make use of Kirchhoff's rules (K1) and (K2) in order to evaluate the diagrams of the relaxation paths. Each diagram and its evaluation is valid for the interval between two main peaks. The solution $\tau^*_{n_1,n_2}$ of the Kirchhoff equations between the peaks $n_1=m_1+m_1'$ and $n_2=m_2+m_2'$ is not written down explicitly, since it is too lengthy and the calculation is straightforward.

(1) $(1/g\mu_B)(A+13B)\leqslant H_z\leqslant(2/g\mu_B)(A+34B)$: From $J=J_1+J_2, J_1=J_3+J_4, J_4=J_5+J_8, J_2+J_5=J_6, J_3+J_6=J_7, J_7+J_8=J$, and $\Delta N=J_1\tau_1+J_3\tau_3+J_7\tau_7, J_3\tau_3=J_4\tau_4+J_5\tau_5+J_6\tau_6, J_2\tau_2=J_1\tau_1+J_4\tau_4+J_5\tau_5, J_8\tau_8=J_5\tau_5+J_6\tau_6+J_7\tau_7$, one can immediately evaluate the relaxation time $\tau^*_{1,2}(H)=\Delta N/J$ (see Figs. 16 and 17).

(2) $(2/g\mu_B)(A+34B)\leqslant H_z\leqslant 3/g\mu_B(A+17B)$: From $J=J_1+J_2, J_1=J_3+J_4+J_7, J_2+J_4=J_5, J_3+J_5=J_6, J_6+J_7=J$, and $\Delta N=J_1\tau_1+J_3\tau_3+J_6\tau_6, J_3\tau_3=J_4\tau_4+J_5\tau_5, J_2\tau_2=J_1\tau_1+J_4\tau_4, J_7\tau_7=J_4\tau_4+J_5\tau_5+J_6\tau_6$, one can immediately evaluate the relaxation time $\tau^*_{2,3}(H)=\Delta N/J$ (see Figs. 18 and 19).

(3) $(3/g\mu_B)(A+17B)\leqslant H_z\leqslant(4/g\mu_B)(A+40B)$: From $J=J_1+J_2, J_1=J_3+J_4, J_4=J_5+J_7, J_2+J_3+J_5=J_6, J_6+J_7=J$, and $\Delta N=J_1\tau_1+J_3\tau_3+J_6\tau_6, J_3\tau_3=J_4\tau_4+J_5\tau_5, J_2\tau_2=J_1\tau_1+J_4\tau_4+J_5\tau_5, J_7\tau_7=J_5\tau_5+J_6\tau_6$, one can immediately evaluate the relaxation time $\tau^*_{3,4}(H)=\Delta N/J$ (see Figs. 20 and 21).

APPENDIX D: FIRST-ORDER vs SECOND-ORDER TRANSITION

We show in this section that second-order transitions lead to a much faster relaxation of the spin system than first-order transitions if the coupling constants are equal. The relaxation rate $\Gamma^{(1)}$ of the cascade with transitions $\Delta m=\pm1$ has been calculated by Villain *et al.*[17] (see Fig. 22),

$$\Gamma^{(1)}=\frac{3}{2\pi}\frac{|V_{1,0}|^2}{\hbar^4\rho c^5}(\varepsilon_0-\varepsilon_1)^3\frac{e^{-\beta\Delta}}{1-e^{-\beta(\varepsilon_0-\varepsilon_1)}}$$
$$=\frac{3}{2\pi}\frac{|V_{1,0}|^2}{\hbar^4\rho c^5}\left[\frac{\Delta}{s^2}\right]^3\frac{e^{-\beta\Delta}}{1-e^{-\beta\Delta/s^2}}. \tag{D1}$$

$\Delta=100A$ is the energy barrier.

We have extended this expression by taking higher-order transitions into account. If we take a cascade with transitions $\Delta m=\pm2$, for the case $s=10$, we obtain

$$\Gamma^{(2)}=\frac{3}{2\pi}\frac{|V_{2,0}|^2}{\hbar^4\rho c^5}(\varepsilon_0-\varepsilon_2)^3\frac{e^{-\beta\Delta}}{1-e^{-\beta(\varepsilon_0-\varepsilon_2)}}$$
$$=\frac{3}{2\pi}\frac{|V_{2,0}|^2}{\hbar^4\rho c^5}\left[\frac{\Delta}{(s/2)^2}\right]^3\frac{e^{-\beta\Delta}}{1-e^{-\beta\frac{\Delta}{(s/2)^2}}}. \tag{D2}$$

Comparing to the relaxation rate $\Gamma^{(1)}$ with $s=10$, an increase by a factor

$$\frac{\Gamma^{(2)}}{\Gamma^{(1)}}\approx\frac{10^6}{5^6}=64 \tag{D3}$$

is obtained, assuming $V^{(1)}\approx V^{(2)}$ (see Abragam and Bleaney,[28] p. 563, for experimental evidence).

Now we calculate the relaxation rate by means of formula (63) with $\Gamma^{(1)}=1/\tau^*$, $\Delta m=\pm1$, and $\Gamma^{(2)}=1/\tau^*$, $\Delta m=\pm2$. If there is a fast transition via tunneling between levels $m=4$ and $m'=-4$ for $H_z=0$ at $T=1.9$ K, we get the following more accurate estimation:

$$\frac{\Gamma^{(2)}}{\Gamma^{(1)}}=11.7. \tag{D4}$$

The same can be done if the fastest transition takes place via tunneling between levels $m=2$ and $m'=-2$ for $H_z=0$ at $T=1.9$ K,

$$\frac{\Gamma^{(2)}}{\Gamma^{(1)}}=49.0. \tag{D5}$$

From these results it is obvious that second-order transitions lead to a faster relaxation. Note that it is Eq. (19) together with Eq. (28) which imply that the ratios (D4) and (D5) are of the same order as the ratio (D3). This provides a theoretical justification for the approximation $V^{(1)}\approx V^{(2)}$.

*Electronic address: Michael.Leuenberger@unibas.ch
†Electronic address: Daniel.Loss@unibas.ch

[1] C. Paulsen and J.-G. Park, in *Quantum Tunneling of Magnetization*, edited by L. Gunther and B. Barbara (Kluwer, Dordrecht, 1995), p. 189.
[2] C. Paulsen, J.-G. Park, B. Barbara, R. Sessoli, and A. Caneschi, J. Magn. Magn. Mater. **140-144**, 379 (1995).
[3] M. A. Novak and R. Sessoli, in *Quantum Tunneling of Magnetization*, edited by L. Gunther and B. Barbara (Kluwer, Dordrecht, 1995), p. 189.
[4] R. Sessoli, D. Gatteschi, A. Caneschi, and M. A. Novak, Nature (London) **365**, 141 (1993).
[5] M. A. Novak, R. Sessoli, A. Caneschi, and D. Gatteschi, J. Magn. Magn. Mater. **146**, 211 (1995).
[6] J. R. Friedman, M. P. Sarachik, J. Tejada, and R. Ziolo, Phys. Rev. Lett. **76**, 3830 (1996).
[7] L. Thomas, F. Lionti, R. Ballou, D. Gatteschi, R. Sessoli, and B. Barbara, Nature (London) **383**, 145 (1996).
[8] J. M. Hernández, X. X. Zhang, F. Luis, J. Bartolomé, J. Tejada, and R. Ziolo, Europhys. Lett. **35**, 301 (1996).
[9] B. Barbara, W. Wernsdorfer, L. C. Sampaio, J. G. Park, C. Paulsen, M. A. Novak, R. Ferré, D. Mailly, R. Sessoli, A. Can-

eschi, K. Hasselbach, A. Benoit, and L. Thomas, J. Magn. Magn. Mater. **140-144**, 1825 (1995).
[10] M. A. Novak and R. Sessoli, in *Quantum Tunneling of Magnetization*, edited by L. Gunther and B. Barbara (Kluwer, Amsterdam, 1995).
[11] J. R. Friedman, M. P. Sarachik, and R. Ziolo, Phys. Rev. B **58**, R14 729 (1998).
[12] F. Luis, J. Bartolomé, and F. Fernández, Phys. Rev. B **57**, 505 (1998).
[13] J. F. Fernández, J. Bartolomé, and F. Luis, J. Appl. Phys. **83**, 181 (1998).
[14] F. Hartmann-Boutron, P. Politi, and J. Villain, Int. J. Mod. Phys. B **10**, 2577 (1996).
[15] W. Wernsdorfer, R. Sessoli, D. Gatteschi, Europhys. Lett. **47**, 254 (1999)
[16] R. Sessoli, Mol. Cryst. Liq. Cryst. Sci. Technol., Sect. A **274**, 145 (1995).
[17] J. Villain, F. Hartmann-Boutron, R. Sessoli, and A. Rettori, Europhys. Lett. **27**, 159 (1994).
[18] A. Fort, A. Rettori, J. Villain, D. Gatteschi, and R. Sessoli, Phys. Rev. Lett. **80**, 612 (1998).
[19] D. A. Garanin and E. M. Chudnovsky, Phys. Rev. B **56**, 11 102 (1997).
[20] L. Gunther, Europhys. Lett. **39**, 1 (1997).
[21] A. L. Barra, D. Gatteschi, and R. Sessoli, Phys. Rev. B **56**, 8192 (1997).
[22] Y. Zhong, M. P. Sarachik, J. R. Friedman, R. A. Robinson, T. M. Kelley, H. Nakotte, A. C. Christianson, F. Trouw, S. M. J. Aubin, and D. N. Hendrickson, J. Appl. Phys. **85**, 5636 (1999).
[23] M. N. Leuenberger and D. Loss, Europhys. Lett. **46**, 692 (1999).
[24] J. M. Hernández *et al.*, Phys. Rev. B **55**, 5858 (1997).
[25] R. Sessoli, H. L. Tsai, A. R. Shake, S. Wang, J. B. Vincent, K. Folting, D. Gatteschi, G. Christou, and D. N. Hendrickson, J. Am. Chem. Soc. **115**, 1804 (1993).
[26] E. Callen and H. Callen, Phys. Rev. **139**, A455 (1965).
[27] V. Dohm and P. Fulde, Z. Phys. B **21**, 369 (1975).
[28] A. Abragam and A. Bleany, *Electron Paramagnetic Resonance of Transition Ions* (Clarendon Press, Oxford, 1970).
[29] K. Blum, *Density Matrix Theory and Applications*, 2nd ed. (Plenum Press, New York, 1996), Chap. 8.
[30] E. Fick and G. Sauermann, *The Quantum Statistics of Dynamic Processes* (Springer, New York, 1990), Chap. 17.
[31] The free propagator within the integral kernel leads to the δ distribution in W_{mn} [see Eq. (27)]. The spin-phonon transition rates (28) are barely affected by the tunnel splitting $E_{mm'}$ [see Eq. (46)], which is smaller than the level spacing $|\varepsilon_m - \varepsilon_{m'}| \geqslant 0.5$ K (see Sec. III B). Therefore the tunneling part $\mathcal{H}_T$ within the integral kernel can be safely omitted.
[32] These expressions are defined in analogy to Eqs. (8.1.24) and (8.1.29) in Ref. 29.
[33] T. Lis, Acta Crystallogr., Sect. B: Struct. Crystallogr. Cryst. Chem. **36**, 2042 (1980).
[34] D. A. Garanin, J. Phys. A **24**, L61 (1991).
[35] L. D. Landau and E. M. Lifschitz, *Quantum Mechanics* (Pergamon, Oxford, 1965).
[36] In the case of spin echoes, the different larmor frequencies within an ensemble of spins cause the decoherence of the system (Ref. 29). As these spins get *smoothly* out of phase, this kind of decoherence is also called dephasing. In the case of the tunneling presented in this work, the coherence of the ensemble of the tunneling spins is destroyed by spin-phonon interactions, which are randomly distributed in time. This means that every time a spin-phonon interaction takes place, one tunneling spin of the ensemble gets abruptly out of phase.
[37] J. Villain *et al.*, J. Phys. I **7**, 1583 (1997).
[38] A similar formula for $\Gamma_m^{m'}$ which has been obtained through a different and more involved derivation (Ref. 37) has been used by Fort *et al.* (Ref. 18).
[39] Note that in Ref. 7 the correct temperature is $T = 1.9$ K, not 2.1 K [B. Barbara and W. Wernsdorfer (private communication)].
[40] I. Mirebeau, M. Hennion, H. Casalta, H. Andres, H. U. Güdel, H. V. Irodova, and A. Caneschi, Phys. Rev. Lett. **83**, 628 (1999).
[41] J. R. Friedman (private communication).
[42] A. M. Gomes, M. A. Novak, R. Sessoli, A. Caneschi, and D. Gatteschi, Phys. Rev. B **57**, 5021 (1998).
[43] N. W. Ashcroft and N. D. Mermin, *Solid State Physics* (Saunders College Publishing, Philadelphia, 1976).
[44] A. Lascialfari, Z. H. Jang, F. Borsa, P. Carretta, and D. Gatteschi, Phys. Rev. Lett. **81**, 3773 (1998).
[45] If one takes tunnel splittings due to higher-order perturbations in B_4 and H_x into account, more but much narrower satellite peaks appear, see T. Pohjola, H. Schoeller, and M. N. Leuenberger, D. Loss (unpublished).
[46] The ratio $W_{m,m+2}/W_{m'-2,m'}$ is approximated by 1. One can see from Eq. (28) that this approximation is well satisfied near a resonance (i.e., within w').
[47] A. Messiah, *Quantum Mechanics* (de Gruyter, New York, 1991).